

FedAPA: Federated Learning with Adaptive Prototype Aggregation Toward Heterogeneous Wi-Fi CSI-based Crowd Counting

Jingtao Guo, *Student Member, IEEE*, Yuyi Mao, *Senior Member, IEEE*,
and Ivan Wang-Hei Ho, *Senior Member, IEEE*

Abstract—Wi-Fi channel state information (CSI)-based sensing provides a non-invasive, device-free approach for tasks such as human activity recognition and crowd counting, but large-scale deployment is hindered by the need for extensive site-specific training data. Federated learning (FL) offers a way to avoid raw data sharing but is challenged by heterogeneous sensing data and device resources. This paper proposes FedAPA, a collaborative Wi-Fi CSI-based sensing algorithm that uses adaptive prototype aggregation (APA) strategy to assign similarity-based weights to peer prototypes, enabling adaptive client contributions and yielding a personalized global prototype for each client instead of a fixed-weight aggregation. During local training, we adopt a hybrid objective that combines classification learning with representation contrastive learning to align local and global knowledge. We provide a convergence analysis of FedAPA and evaluate it in a real-world distributed Wi-Fi crowd counting scenario with six environments and up to 20 people. The results show that our method outperform multiple baselines in terms of accuracy, F1 score, mean absolute error (MAE), and communication overhead, with FedAPA achieving at least a 9.65% increase in accuracy, a 9% gain in F1 score, a 0.29 reduction in MAE, and a 95.94% reduction in communication overhead.

Index Terms—Federated learning (FL), Wi-Fi sensing, crowd counting, representation learning, device heterogeneity.

I. INTRODUCTION

WI-FI sensing technologies have seen widespread use in various fields, including indoor positioning [1] and crowd counting [2]. Among these applications, crowd counting is crucial for optimizing space allocation in restaurants, transportation hubs, and public facilities, and for improving energy efficiency through automatic control of air conditioning and electrical systems. Current crowd counting methods fall into two categories: device-based and device-free approaches [3]. Device-based methods require each individual in the crowd to carry a sensor [4], which is often inconvenient or infeasible. Device-free methods are further divided into sensor-based, image-based, and radio frequency (RF)-based counting. Sensor-based methods (e.g., CO₂, acoustic, LiDAR, infrared) require additional infrastructure, increasing deployment costs. Image-based techniques, although widely used [5], raise privacy concerns and are sensitive to non-line-of-sight (NLOS) and lighting conditions, which limits their applicability in many indoor and outdoor scenarios [6]. RF-based systems, using signals such as Bluetooth and Wi-Fi, offer a contactless and

NLOS-capable alternative, with Wi-Fi-based methods being particularly attractive due to their low cost and widespread availability [7].

Wi-Fi signal scattering and reflection vary with the number of people in an indoor space, forming useful patterns for crowd counting and occupancy detection. The two main radio signal features used for human activity sensing are the received signal strength indicator (RSSI) and channel state information (CSI) matrix [3], [6]. While RSSI-based crowd counting techniques have shown potential [8], they fail to meet the robustness and scalability requirements for accurate real-world occupancy measurement due to distortion caused by multi-path fading [3], [9]. In contrast, the CSI matrix provides amplitude and phase information across multiple sub-carriers, is able to capture subtle environmental changes, making it a great choice for crowd counting [7], [10], [11].

Several CSI-based occupancy measurement systems [2], [12]–[15] use support vector machines (SVM), long short-term memory (LSTM) networks, and convolutional neural networks (CNN) to estimate the number of people in a target area. However, these models are typically trained in isolation for each environment, which limits scalability in large deployments. A natural idea is to aggregate CSI data from many devices for centralized cloud training, but sharing Wi-Fi sensing data across environments and ownership domains introduces serious privacy and security risks [16]. For example, attackers can generate adversarial CSI samples using jamming signals based on normal CSI data, causing incorrect or even malicious model outputs [17]. Moreover, edge devices usually have limited computation due to low-cost and low-power constraints. Offloading raw CSI to the cloud for centralized processing is also problematic: the high dimensionality and sampling rate of CSI create a continuous data stream that can saturate communication bandwidth and interfere with basic WiFi services (e.g., Internet access). Therefore, an efficient distributed algorithm is needed to reduce communication overhead while preserving sensing accuracy.

Federated learning (FL) allows multiple edge devices or organizations to collaboratively train a global model without sharing raw data, coordinated by a central server [18]. However, deploying FL in distributed Wi-Fi sensing systems is challenged by statistical and model heterogeneity. CSI data from different environments are typically non-independent and identically distributed (non-IID), and edge devices have varying computational resources, making it difficult to learn a single global

model [19], [20]. For example, meeting rooms and offices exhibit different propagation and occupancy patterns, while hardware ranges from laptops with Intel 5300 NICs to resource-constrained ESP-32 modules, which call for different model architectures. Consequently, naive strategies such as simple model averaging are often insufficient to obtain an effective global model across such heterogeneous environments and devices.

To address these challenges, researchers have proposed various modifications to local training and global aggregation within the FedAvg framework [21]. For example, MOON [22] incorporated global model knowledge into local training to reduce the drift of local updates, guiding the update of the global model toward an unbiased trajectory. Another common strategy involved sharing prototypes (the mean of feature embeddings for each label) to regularize local training [23]. However, these existing methods are often limited by either focusing on addressing a single type of heterogeneity or achieving only marginal performance improvements, making them less effective for clients with diverse data and resource distributions, particularly in scenarios where some clients possess data from only a few classes [24].

This paper aims to address the challenges of statistical and model heterogeneity, including feature-skew, label-skew, and diverse model architectures, which commonly arise in distributed Wi-Fi people-counting applications. Specifically, we introduce a novel FL algorithm, FedAPA, which promotes collaboration across clients with similar data distributions by adaptive prototype aggregation (APA) module. The main contributions of this paper are five-fold:

- We present **FedAPA**, a FL algorithm for distributed Wi-Fi CSI crowd counting that handles both statistical heterogeneity (non-IID data) and model heterogeneity. FedAPA coordinates clients through class prototypes while keeping per-client personalization.
- We design an APA module that weights and aggregates client prototypes by similarity. This enables knowledge sharing among similar clients and reduce communication overhead by exchanging compact prototypes instead of gradients or full models.
- We introduce a hybrid local objective that aligns local and global knowledge by combining cross entropy with a prototype contrastive loss (PCL). A warm-up schedule gradually increases the PCL weight to avoid early instability and reduce drift between local and global representations.
- We present a convergence analysis of the proposed algorithm and derive a nonconvex convergence rate, highlighting how prototype similarity-aware aggregation and warm-up strategies affect convergence.
- We validate FedAPA on a real-world Wi-Fi CSI crowd-counting dataset across multiple architectures and non-IID splits. FedAPA consistently outperforms several FL-based Wi-Fi sensing baselines while lowering client-side communication overhead, showing practical gains for resource-constrained deployments.

The remainder of this paper is structured as follows: Section II reviews related works, providing the literature context for

TABLE I
KEY NOTATIONS USED IN THIS ARTICLE.

Symbol	Meaning
N	Number of clients (Wi-Fi devices).
$\mathcal{C}, \mathcal{C}_i$	Global label set; labels present at client i .
$\mathcal{D}_i, \mathcal{D}_i^c$	Dataset at client i ; class- c subset at client i .
$w_i = (w_i^\theta, w_i^h)$	Encoder and classifier parameters of client i .
$\mathbf{r}_i(\mathbf{h})$	Embedding of CSI input \mathbf{h} at client i .
$\mathbf{p}_i^c, \mathbf{P}_i$	Class- c prototype; prototype set of client i .
\mathbf{P}	Stacked prototype sets of all clients.
$\mathbf{q}_i^c, \mathbf{Q}_i$	Personalized class- c prototype; personalized set for client i .
τ	Temperature for aggregation and contrastive logits.
λ	Weight of prototype-based losses.
$S, T, K=TS$	Local SGD steps per round; rounds; total local steps.
η	Learning rate for local updates.
$\mathcal{L}_{ce}, \mathcal{L}_g, \mathcal{L}_c, \Phi$	Cross-entropy loss; contrastive loss w.r.t. \mathbf{Q}_i ; contrastive loss w.r.t. \mathbf{P} ; combined prototype regularizer.
L_{\max}, σ^2, G	Smoothness bound after warm-up; gradient-variance bound; bound on $\mathbb{E}\ g_{i,t,s}\ ^2$.
$G_{i,t}$	Sum of gradient norms across S local steps at round t for client i .
k_{glob}	Prototype-movement constant in the convergence bounds.
$\Gamma(\tau)$	Sensitivity term in prototype-refresh error, $\Gamma(\tau) = c_\Phi(\tau)(1 + L_{\text{agg}}(\tau))$.
L_{inf}, Δ_i	Lower bound on local objectives; initial gap for client i after warm-up.

our proposed method. Section III introduces CSI background and outlines the problem statement. Section IV presents our proposed federated learning algorithm. Section V provides a convergence analysis of our proposed approach. Section VI describes the experimental setup and results. Section VII and VIII conclude with a summary of findings and contributions.

II. RELATED WORKS

A. Wi-Fi CSI-Based crowd Counting System

Recent advancements in Wi-Fi CSI-based crowd counting systems [25], [26] have aimed to address the challenge of data distribution shifts when pretrained models are deployed in new environments. However, many models still require additional fine-tuning to achieve optimal performance in new environments. With the emergence of 6G technology, it is now possible to aggregate large amounts of data from diverse environments, enabling the training of a Wi-Fi sensing foundation model.

B. Collaborative Wi-Fi-based Sensing System

Federated learning (FL) trains Wi-Fi sensing models across edge devices without sharing raw CSI by using on-device updates and server-side aggregation. In Wi-Fi sensing, FL has been applied to handle non-IID data: CARING [27] reweights client updates by local performance to improve cross-domain recognition, and WiFederated [28] scales training across multiple locations. However, these methods often need extra training rounds or yield limited gains under strong non-IID conditions. To reduce labeling costs, Zhang et al. [29] propose a cross-domain FL framework that synthesizes wireless-like data

from images and uses MMD-based domain adaptation, adding transfer and adaptation overhead. Liu et al. [30] introduce a vertical Federated Edge Learning (FEEL) framework that exchanges low-dimensional intermediate features for collaborative object and motion recognition while protecting raw data, but it mainly addresses feature-partitioned settings rather than label skew. In contrast, our approach targets label skew, feature skew, and resource limits jointly, and reduces communication by sharing and aggregating class prototypes instead of full models.

C. Personalized FL

To handle statistical heterogeneity in data and models, personalized FL (pFL) methods aim to learn client-specific models rather than a single global one. Instead of only optimizing a centralized model via distributed training, pFL explicitly tailors each client's model to its local data and, when needed, architecture. These methods are commonly grouped into three categories:

- 1) **Global model with local fine-tuning**, as in WiFederated [28], which first trains a shared model and then adapts it on each client.
- 2) **Personalized layers or representations**, such as FedRep [31], which shares a common encoder and trains local heads; FedBN [32], which keeps batch normalization layers local to mitigate feature shift; and FedProto [23], which exchanges class prototypes instead of model parameters to support heterogeneous architectures.
- 3) **Personalized aggregation**, which builds local models from client-dependent combinations of global and local parameters, for example FedALA [33] with element-wise aggregation and FedAMP [34] with similarity-weighted aggregation of client models.

FedAPA belongs to class (2): it communicates and aggregates class prototypes through an APA module, so clients share compact class summaries while keeping their local models and statistics private.

III. PRELIMINARIES AND PROBLEM STATEMENT

In this section, we first briefly introduce Wi-Fi CSI, it is then followed by the formulation of a general prototype-based FL framework for Wi-Fi CSI-based crowd counting.

A. Wi-Fi CSI

Wi-Fi technologies utilize orthogonal frequency division multiplexing (OFDM), where data and reference symbols are transmitted via S_{sub} orthogonal subcarriers. Wi-Fi CSI represents the estimated channel response between a Wi-Fi transmitter (Tx) and a receiver (Rx) for each subcarrier. This information is readily available at the receiver and can be extracted using CSI extraction middlewares such as Nexmon CSI extractor [35] Assuming K_{pkt} data packets are transmitted by a Wi-Fi transmitter with N_t antennas to a receiver with N_r antennas, each Wi-Fi CSI sample is represented as a tensor with dimensions $N_t \times N_r \times K_{pkt} \times S_{sub}$. The channel coefficient



(a) Living room scenario (b) Conference room scenario

Fig. 1. Illustration of two different environment layout for Wi-Fi CSI-based crowd counting data collection.

between the n_t -th transmit antenna and n_r -th receive antenna for the k -th packet at subcarrier s is expressed as:

$$h_{k,s}^{n_t, n_r} = |h_{k,s}^{n_t, n_r}| e^{j \cdot \theta_{k,s}^{n_t, n_r}}, \quad (1)$$

where $|h_{k,s}^{n_t, n_r}|$ and $\theta_{k,s}^{n_t, n_r}$ represent the amplitude and phase coefficients, respectively. The label of each Wi-Fi CSI sample, y , indicates the number of people present.

Consider two scenarios, each with a Wi-Fi transmitter-receiver pair, as shown in Fig. 1 (a) and (b). Each environment, such as a conference room versus a living room, has unique properties that cause variations in signal characteristics. The challenge lies in training models that generalize well across different environments without extensive data collection. A model trained in one environment may not perform well in another, necessitating the design of a collaborative training framework that shares knowledge across environments to improve generalization and reduce the need for data collection.

B. Prototype-based FL for Wi-Fi CSI-based crowd Counting

FL leverages Wi-Fi CSI data from multiple environments to learn crowd counting models. Standard FL methods, such as FedAvg [21], train a single shared model across N clients (Wi-Fi receivers in different environments). In practice, Wi-Fi CSI-based crowd counting is highly non-IID: people density and movement patterns vary across spaces (for example, a busy shopping mall on weekends versus an office after hours), and receivers also differ in computational resources. As a result, a single global model is often suboptimal, and personalized models tailored to each environment are needed.

We conceptualize a client model w_i as the combination of an encoder w_i^e and a classifier w_i^c . The embedding of the l -th Wi-Fi CSI matrix with label y at client i , denoted $\mathbf{h}_i^{l,y}$, is computed as $\mathbf{r}(\mathbf{h}_i^{l,y}) \triangleq f_i(\mathbf{h}_i^{l,y}; w_i^e)$, and the prediction is given by $g_i(\mathbf{r}(\mathbf{h}_i^{l,y}); w_i^c)$. Each client will then generate its prototype for each class c as $\mathbf{p}_i^c \triangleq \frac{1}{|\mathcal{D}_{i,c}|} \sum_{l=1, y \in c}^{|\mathcal{D}_{i,c}|} \mathbf{r}_i^{l,y}$ at the t -th communication round, where $\mathcal{D}_{i,c} = \{(\mathbf{h}, y) \in \mathcal{D}_i : y = c\}$, and $|\mathcal{D}_{i,c}|$ is the number of samples of class c for client i . The client collaboration involves sharing their prototypes with a central server and generating global prototypes \mathbb{P} for each client, which brings external information to other clients. The original prototype-based FL algorithm for Wi-Fi CSI-based crowd counting is formulated as:

$$\min_{w_1, w_2, \dots, w_N} \frac{1}{N} \sum_{i=1}^N \mathbb{E}_{(\mathbf{h}, y) \in \mathcal{D}_i} [\mathcal{L}(\mathbf{h}, y, \mathbb{P}; w_i)], \quad (2)$$

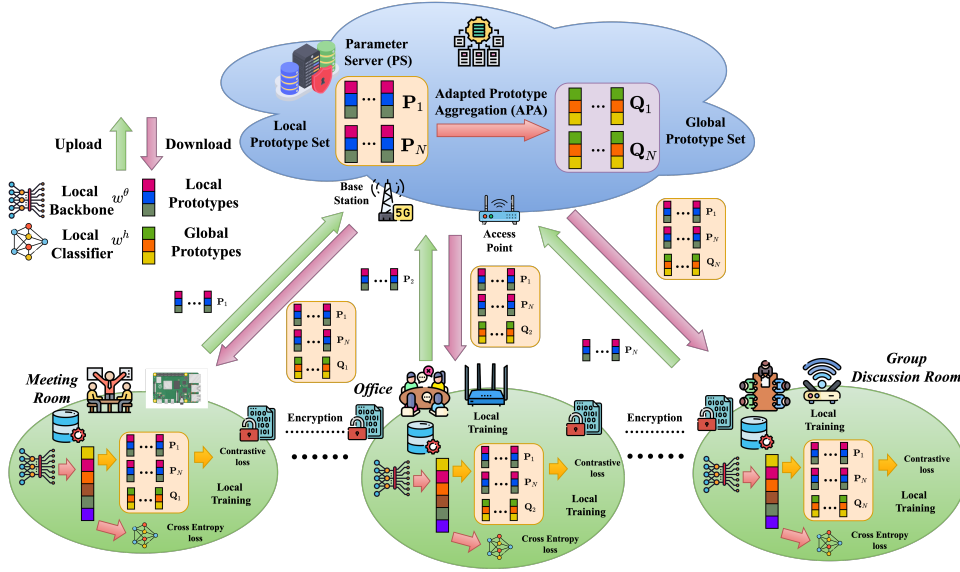


Fig. 2. Overview of the proposed framework. **Bottom:** Clients with varying computational resources capture CSI data in distinct environments (e.g., Meeting Room, Office) and extract local prototypes from CSI data. **Top:** The Parameter Server aggregates uploads via Adapted Prototype Aggregation (APA) to form personalized sets \mathbf{Q} . **Training:** Clients optimize backbones w^θ and classifiers w^h using the returned global \mathbf{P} and personalized \mathbf{Q} sets via a hybrid loss.

with the local loss function \mathcal{L} defined as

$$\mathcal{L}(\mathbf{h}, y, \mathbb{P}; w_i) = \mathcal{L}_{ce}(g_i(f_i(\mathbf{h}; w_i^\theta); w_i^h), y) + \lambda \mathcal{L}_g(f_i(\mathbf{h}; w_i^\theta), \mathbb{P}), \quad (3)$$

where $\mathcal{L}_{ce}(\cdot, \cdot)$ is the cross-entropy loss for classification, $\mathcal{L}_g(\cdot, \cdot)$ is a representation learning loss that aligns local embeddings with global prototypes, and λ is a hyperparameter balancing the two loss components. Here, N is the total number of clients, \mathcal{D}_i is the local dataset of client i , and \mathbb{P} is the global prototypes that average clients' uploaded prototype set. In our proposed algorithm, we replace \mathbb{P} by personalized global prototypes \mathbf{Q}_i built by similarity-aware aggregation, and add an inter-client loss term that leverages the whole uploaded prototypes $\mathbf{P} = \{\mathbf{P}_i\}_{i=1}^N$. Details of \mathbf{Q}_i generation and the local training procedure are described in Section IV.

IV. FEDAPA

This section presents the FedAPA framework, illustrated in Fig. 2. We consider multiple crowd counting environments connected to a parameter server (PS). FedAPA introduces a prototype-based aggregation scheme inspired by prototype learning [36], which fuses feature representations from heterogeneous data by aggregating class-wise embeddings. Unlike prior prototype-based FL methods [23], [37], [38] that form a single global prototype via uniform averaging, FedAPA constructs personalized global prototypes based on inter-client similarity. Each client receives its personalized prototypes and the full prototype set from the PS, and trains a local model with a hybrid loss that combines classification and prototype-wise contrastive learning. This aligns global and local representations and strengthens inter-client knowledge sharing in the latent space. The following subsections detail the three components of FedAPA: **Prototypes as compact information carriers**, **Server aggregation**, and **Local training**.

A. Prototypes as compact information carriers

In Wi-Fi sensing task, raw CSI amplitude matrix is usually high-dimensional, making direct sharing across clients impractical due to communication constraints. To enhance client-specific knowledge sharing while reducing the communication overhead, we leverage a prototype-based information-sharing strategy. By exchanging prototypes per client, the communication cost is far smaller than pushing full models or sharing raw CSI streams. Because prototypes are computed from the information of last round, they carry fresh information forward without exposing raw CSI. At t -th round, each client i updates its local model $w_{i,t}$ on \mathcal{D}_i and maps each CSI matrix \mathbf{h} to an embedding $\mathbf{r}_i(\mathbf{h}; w_{i,t})$. For every class c , the client forms a prototype as its mean embedding:

$$\mathbf{p}_{i,t}^c := \frac{1}{m_i^c} \sum_{\mathbf{h} \in \mathcal{D}_i^c} \mathbf{r}_{w_{i,t}, S}^\theta(\mathbf{h}), \quad m_i^c := |\mathcal{D}_i^c| \geq 1. \quad (4)$$

Once its local prototype set \mathbf{P}_i is constructed, the client uploads it to the PS for aggregation, facilitating client-specific compact information sharing derived from local datasets.

B. Server aggregation

After receiving the prototype set \mathbf{P} , the PS first computes pairwise inter-client cosine similarity [34], [39] using prototypes of each class as follows:

$$s_{ij}^c = \frac{(\mathbf{p}_i^c)^\top \mathbf{p}_j^c}{\|\mathbf{p}_i^c\|_2 \|\mathbf{p}_j^c\|_2}, \quad c \in (\mathcal{C}_i \cap \mathcal{C}_j), \quad (5)$$

where \mathbf{p}_i^c and \mathbf{p}_j^c are the prototypes of class c of the i -th and j -th clients, respectively. Let $\mathcal{J}_c(i) := \{j : c \in (\mathcal{C}_i \cap \mathcal{C}_j)\}$ be the eligible client set for client i with class c . It then generates an adaptive weight α_{ij}^c of each class with softmax normalization:

$$\alpha_{ij}^c = \frac{\exp(s_{ij}^c/\tau)}{\sum_{j \in \mathcal{J}_c(i)} \exp(s_{ij}^c/\tau)}, \quad (6)$$

where τ is the temperature hyperparameter used to sharpen the distribution. Instead of fixed or uniform weights, the adaptive weights α_{ij}^c allow each client aggregates class-wise prototypes mainly from similar peers. This adaptive weighting strategy reduces negative transfer from heterogeneous clients [34], [40] and produces client-specific prototype sets instead of a single global average. In our convergence analysis (Section V), the effect of similarity-weighted aggregation is captured by a Lipschitz constant $\Gamma(\tau)$ that depends on the softmax temperature τ , and enters the bounds through the cross-client coupling term $\lambda\Gamma(\tau)k_{\text{glob}}G$. With the normalized weights, the server aggregates the prototypes of class c for client i as

$$\mathbf{q}_i^c = \sum_{j \in \mathcal{J}_c(i)} \alpha_{ij}^c \mathbf{p}_j^c. \quad (7)$$

After aggregation for all clients, the server returns the global personalized prototypes $\mathbf{Q}_i := \{\mathbf{q}_i^c\}_{c \in \mathcal{C}_i}$ to client i . To handle clients with missing classes and stabilize prototype-based collaboration under label-skew non-IID distributions, we adopt a prototype padding mechanism. For any class \hat{c} absent at client i , we construct a pseudo-prototype for \mathbf{Q}_i and \mathbf{P}_i by sample-weighted averaging of the corresponding prototypes from other clients, i.e.,

$$\mathbf{p}_i^{\hat{c}} = \mathbf{q}_i^{\hat{c}} = \frac{1}{|\mathcal{J}_{\hat{c}}|} \sum_{j \in \mathcal{J}_{\hat{c}}} \mathbf{p}_j^{\hat{c}}, \quad (8)$$

where $\mathcal{J}_{\hat{c}} := \{j : \hat{c} \in \mathcal{C}_j, \hat{c} \notin \mathcal{C}_i\}$, and include this padded prototype in our contrastive representation learning. This yields a complete, globally consistent prototype set for each client, while simultaneously providing informative negative anchors in the contrastive loss for classes that are not observed locally, thereby improving cross-client feature alignment without sharing raw data. This approach promotes stronger collaboration among clients with similar data distributions while reducing computational costs compared to methods like FedAMP [34], which rely on model parameters for collaboration. Unlike approaches such as [23], [37], [38] that average uploaded prototypes directly, our method iteratively assigns weights to clients with similar prototypes during aggregation. This process creates a positive feedback loop that strengthens collaboration among similar clients. Furthermore, it dynamically forms cohorts of similar clients, enhancing the overall effectiveness of collaboration. Apart from the global personalized prototypes, each client will also receive the full uploaded prototype set \mathbf{P} .

C. Local training

Upon receiving aggregated prototype \mathbf{Q}_i and client prototypes $\mathbf{P}_{\mathcal{J}_i}$ from the PS, the primary objective of local training is to effectively mitigate the divergence caused by local updates while extracting both class-relevant and inter-client representational knowledge. To achieve this, we propose a hybrid learning architecture that utilizes a warm-up coefficient to integrate classifier learning with representation contrastive learning. Figure 3 illustrates the local training process for each client. To encourage $\mathbf{r}_i(\mathbf{h})$ extracted by local encoder to better align with its corresponding aggregated prototype so that it can learn more class-relevant and client-irrelevant knowledge,

we introduce a global personalized prototype-based contrastive loss term, \mathcal{L}_g , as defined below:

$$\mathcal{L}_g = \mathbb{E}_{(\mathbf{h}, y) \in \mathcal{D}_i} \left[-\log \frac{\exp\left(\frac{\cos(\mathbf{r}_i(\mathbf{h}), \mathbf{q}_i^y)}{\tau}\right)}{\sum_{\hat{y} \in \mathcal{C}} \exp\left(\frac{\cos(\mathbf{r}_i(\mathbf{h}), \mathbf{q}_i^{\hat{y}})}{\tau}\right)} \right]. \quad (9)$$

This contrastive loss function is designed to align the client's local representation to its corresponding global personalized prototype. This helps to reduce the discrepancy between local and global knowledge updates. Cosine similarity is used to compute the distance among global compact embedding and current local compact.

Apart from aligning global knowledge, to enable the local model to learn more inter-client knowledge, we also define a local prototype-based loss term, \mathcal{L}_c , as follows:

$$\mathcal{L}_c = \frac{1}{N} \sum_{j \in N} \mathbb{E}_{(\mathbf{h}, y) \in \mathcal{D}_i} \left[-\log \frac{\exp\left(\frac{\cos(\mathbf{r}_i(\mathbf{h}), \mathbf{p}_j^y)}{\tau}\right)}{\sum_{\hat{y} \in \mathcal{C}} \exp\left(\frac{\cos(\mathbf{r}_i(\mathbf{h}), \mathbf{p}_j^{\hat{y}})}{\tau}\right)} \right]. \quad (10)$$

In addition to the representation learning terms, we also define a classification term, denoted as \mathcal{L}_{ce} , which employs a cross-entropy function for classifier learning.

To stabilize training and guide the model through a logical progression of learning stages, preventing it from being overwhelmed by complex objectives too early, we introduce a warm-up coefficient λ inspired by curriculum learning [41]. It is defined as

$$\lambda = \lambda_{\min} + \frac{(\lambda_{\max} - \lambda_{\min})}{2} (1 - \cos(\pi \cdot u_t)), \quad (11)$$

$$u_t = \frac{\min(t, T_{\text{warm}})}{T_{\text{warm}}},$$

where λ_{\min} and λ_{\max} are the minimum and maximum values of λ , t represents the t -th communication round, while the hyperparameter T_{warm} controls the length of the representation learning warm-up phase. When $t \geq T_{\text{warm}}$, $\lambda_t \equiv \lambda_{\max}$. The default values of λ_{\min} , λ_{\max} , and T_{warm} are set to zero, one, and 50, respectively.

At the early stage, λ is close to zero. The total loss is therefore dominated by the cross-entropy term \mathcal{L}_{ce} . Hence, the model's first and most important job is to learn the basics of the classification task. By focusing almost exclusively on cross-entropy, the model learns the coarse high-level decision boundaries. As training progresses, λ smoothly increases from zero to one through cosine-based scheduler. The contrastive loss terms \mathcal{L}_g and \mathcal{L}_c become more and more influential. This curriculum introduces the harder task for the model learning: organizing the feature space. This feature organizing pressure from the contrastive loss forces the model to build a more robust, meaningful, and generalizable understanding of the feature from both local and global knowledge. By the time λ reaches its maximum value, the model is being trained to do both jobs simultaneously: classify correctly and maintain a well-structured internal representation. The total loss for client

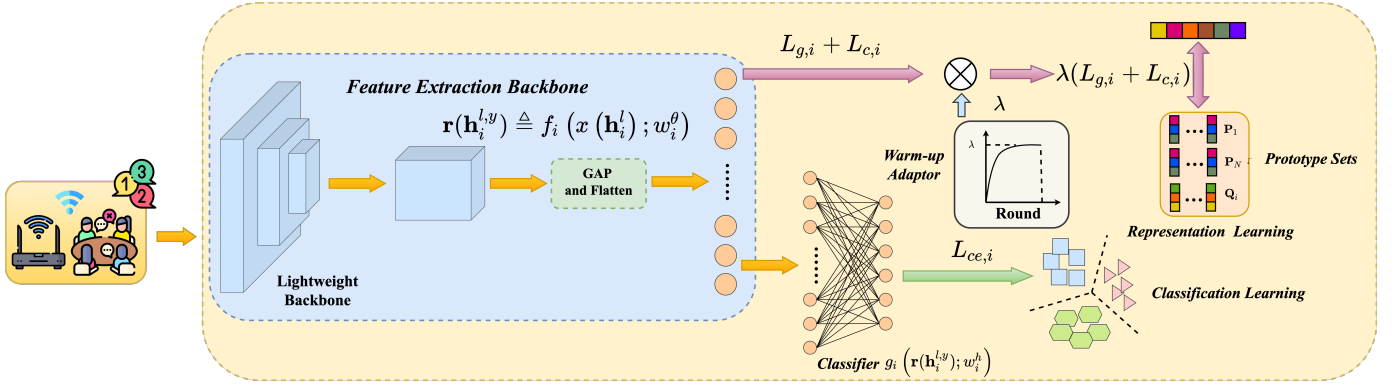


Fig. 3. The encoder w_i^θ extracts features \mathbf{r}_i from CSI input \mathbf{h} for classification by w_i^h . The training objective integrates cross-entropy with contrastive alignment against prototype sets \mathbf{Q}_i and \mathbf{P} , modulated by a warm-up coefficient λ that progressively emphasizes representation learning after classification stabilizes.

Algorithm 1 Server

Require: Clients $i = \{1, \dots, N\}$, rounds T

- 1: Initialize prototype set $\mathbf{P}_{i,0}$ and $\mathbf{Q}_{i,0}$ for each client i
- 2: **for** $t = 1$ to T **do**
- 3: **for** each client i in parallel **do**
- 4: $\mathbf{P}_{i,t} \leftarrow \text{ClientUpdate}(i, \mathbf{Q}_{i,t-1}, \mathbf{P}_{t-1})$
- 5: **for** each $c \in \mathcal{C}_i$ with $c \in \mathcal{C}_j$ **do**
- 6: Compute cosine similarity s_{ij}^c by Eq. (5)
- 7: Convert to weights α_{ij}^c by Eq. (6)
- 8: Form $\mathbf{q}_{i,t}^c$ by Eq. (7)
- 9: **end for**
- 10: Update $\mathbf{Q}_{i,t} \leftarrow \{\mathbf{q}_{i,t}^c\}_{c \in \mathcal{C}_i}$
- 11: Pad missing prototypes in $\mathbf{Q}_{i,t}$ and $\mathbf{P}_{i,t}$ by Eq. (8)
- 12: **end for**
- 13: **Return** to each client i : $\mathbf{Q}_{i,t}$ and the fully uploaded prototype sets \mathbf{P}_t
- 14: **end for**

i is computed by combining the weighted representation loss terms, $\lambda(\mathcal{L}_g + \mathcal{L}_c)$ and \mathcal{L}_{ce} , through addition, as shown below:

$$\mathcal{L}(\mathcal{D}_i, w_i) = \mathcal{L}_{ce}(w_i) + \lambda(\mathcal{L}_g(w_i; \mathbf{Q}_i) + \mathcal{L}_c(w_i; \mathbf{P})). \quad (12)$$

Eq. (12) modifies the original prototype-based FL loss Eq. (3) by: (i) replace the general global prototype \mathbb{P} with the personalized global prototype \mathbf{Q}_i ; (ii) add additional inter-client prototype learning loss; (iii) using warm-up schedule for λ . After finishing local training of each communication round, all clients will upload their prototype sets to the PS for the next round.

V. CONVERGENCE ANALYSIS

We summarize the main theoretical guarantees of FedAPA in this section, and refer to existing works [23], [42]–[44] for the following assumptions and results.

A. Assumptions

We assume full participation and let $L_{\text{inf}} \in \mathbb{R}$ be a uniform lower bound for all local objectives.

Algorithm 2 ClientUpdate($i, \mathbf{Q}_{i,t-1}, \mathbf{P}_t - 1$)

Require: Local dataset \mathcal{D}_i ; model w_i ; steps S ;

- 1: Receive $\mathbf{Q}_{i,t-1}$, and \mathbf{P}_{t-1}
- 2: Update warm-up coefficient λ_t by Eq. (11)
- 3: **for** $s = 1$ to S **do**
- 4: **for** each batch (\mathbf{h}, y) in \mathcal{D}_i **do**
- 5: Compute \mathcal{L}_g by Eq. (9) with personalized global prototypes $\mathbf{Q}_{i,t-1}$
- 6: Compute \mathcal{L}_c by Eq. (10) using fully uploaded prototype sets \mathbf{P}_{t-1}
- 7: Update $w_{i,t}$ by Eq. (12)
- 8: **end for**
- 9: **end for**
- 10: Build local prototypes $\mathbf{p}_{i,t}^c$ for each $c \in \mathcal{C}_i$ by Eq. (4) to form $\mathbf{P}_{i,t}$
- 11: **return** $\mathbf{P}_{i,t}$ to the server

Assumption 1 (Smoothness and lower boundedness). For each round t and client i , the local objective $\mathcal{L}_{i,t}$ in (12) has L_t -Lipschitz gradient:

$$\|\nabla \mathcal{L}_{i,t}(u) - \nabla \mathcal{L}_{i,t}(v)\| \leq L_t \|u - v\|, \quad \forall u, v, \quad (13)$$

with

$$L_t = L_{ce} + \lambda_t L_\Phi, \quad L_t \leq L_{\text{max}} := L_{ce} + \lambda L_\Phi \quad (14)$$

after warm-up. Moreover,

$$\mathcal{L}_{i,t}(w) \geq L_{\text{inf}} \quad \forall i, t, w. \quad (15)$$

Assumption 2 (Stochastic gradients). For client i , round t , and local step s , the stochastic gradient $g_{i,t,s}$ satisfies

$$\mathbb{E}[g_{i,t,s} \mid w_{i,t,s}] = \nabla \mathcal{L}_{i,t}(w_{i,t,s}), \quad (16)$$

$$\mathbb{E}\|g_{i,t,s} - \nabla \mathcal{L}_{i,t}(w_{i,t,s})\|^2 \leq \sigma^2, \quad (17)$$

for some $\sigma^2 \geq 0$, uniformly over all i, t, s . In addition, there exists $G > 0$ such that

$$\mathbb{E}\|g_{i,t,s}\|^2 \leq G^2 \quad \text{for all } i, t, s. \quad (18)$$

Assumption 3 (Bounded and Lipschitz representations). Encoder outputs are uniformly bounded:

$$\|\mathbf{r}_{w^\theta}(\mathbf{h})\| \leq 1 \quad \text{for all } w^\theta, \mathbf{h}, \quad (19)$$

so all prototypes (original and padded) satisfy $\|\mathbf{p}_{i,t}^c\| \leq 1$. The encoder is Lipschitz in its parameters: there exists $L_{w^\theta} > 0$ such that

$$\|\mathbf{r}_{w^\theta}(\mathbf{h}) - \mathbf{r}_{\hat{w}^\theta}(\mathbf{h})\| \leq L_{w^\theta} \|w^\theta - \hat{w}^\theta\|, \quad \forall w^\theta, \hat{w}^\theta, \mathbf{h}.$$

Assumption 4 (Lipschitz personalized aggregation). *Let \mathbf{P} be the stacked local prototypes, and let $\mathbf{Q}_\tau(\mathbf{P})$ be the similarity-weighted aggregation in Section IV-B. There exists $L_{\text{agg}}(\tau) > 0$ such that*

$$\|\mathbf{Q}_\tau(\mathbf{P}) - \mathbf{Q}_\tau(\mathbf{P}')\|_F \leq L_{\text{agg}}(\tau) \|\mathbf{P} - \mathbf{P}'\|_F \quad \forall \mathbf{P}, \mathbf{P}'. \quad (20)$$

Assumption 5 (Prototype regularizer). *For each client i , the prototype-based regularizer $\Phi_i(w; \mathbf{Q}, \mathbf{P})$ is Lipschitz in (\mathbf{Q}, \mathbf{P}) and uniformly bounded: there exist $c_\Phi(\tau) > 0$ and $B_\Phi > 0$ such that*

$$|\Phi_i(w; \mathbf{Q}, \mathbf{P}) - \Phi_i(w; \mathbf{Q}', \mathbf{P}')| \leq c_\Phi(\tau) (\|\mathbf{Q} - \mathbf{Q}'\|_F + \|\mathbf{P} - \mathbf{P}'\|_F), \quad (21)$$

$$0 \leq \Phi_i(w; \mathbf{Q}, \mathbf{P}) \leq B_\Phi, \quad (22)$$

for all $w, \mathbf{Q}, \mathbf{P}, \mathbf{Q}', \mathbf{P}'$.

Assumption 6 (Warm-up schedule). *The weights $\{\lambda_t\}_{t \geq 1}$ are nondecreasing and there exist $T_{\text{warm}} < \infty$ and $\lambda \geq 0$ such that*

$$\lambda_t = \lambda \quad \text{for all } t \geq T_{\text{warm}}. \quad (23)$$

For each client i and round t , we define the within-round gradient norm

$$G_{i,t}^2 := \sum_{s=0}^{S-1} \mathbb{E}[\|\nabla \mathcal{L}_{i,t}(w_{i,t,s})\|^2]. \quad (24)$$

We also define

$$\Gamma(\tau) := c_\Phi(\tau)(1 + L_{\text{agg}}(\tau)), \quad (25)$$

and denote by k_{glob} the prototype-movement constant from Lemma 2(b) in Appendix A.

B. Convergence results

Based on the above assumptions, we have the following convergence result for an arbitrary client in FedAPA.

Theorem 1 (One-round deviation for an arbitrary client). *Let Assumptions 1 to 5 hold. For any client i and any t , with step size $0 < \eta \leq 1/L_t$, we have*

$$\begin{aligned} \mathbb{E}[\mathcal{L}_{i,t+1}(w_{i,t+1,0})] &\leq \mathbb{E}[\mathcal{L}_{i,t}(w_{i,t,0})] - \frac{\eta}{2} G_{i,t}^2 \\ &\quad + \frac{L_t \eta^2}{2} S \sigma^2 + \lambda_{t+1} \Gamma(\tau) k_{\text{glob}} \eta S G \\ &\quad + |\lambda_{t+1} - \lambda_t| B_\Phi. \end{aligned} \quad (26)$$

Under Assumptions 1 to 5, Theorem 1 bounds the one-round change of any client's objective as a descent term, proportional to the squared gradient norm, minus three error terms: a stochastic-variance term, a prototype-refresh term of order $\lambda_{t+1} \Gamma(\tau) k_{\text{glob}} \eta S G$, and a schedule-change term of order $|\lambda_{t+1} - \lambda_t| B_\Phi$. When η , λ_t , and τ are chosen so that these errors are smaller than the descent term, the expected objective of each client is nonincreasing up to $O(\eta^2)$ and prototype-refresh fluctuations. Similarity-weighted aggregation and the warm-up

schedule affect per-round descent only through $\Gamma(\tau)$, k_{glob} , and λ_t , which is consistent with standard nonconvex SGD analyses and prototype-based FL results; intuitively, smoother or similarity-aware aggregation can reduce $\Gamma(\tau)$ and thus relax the per-round descent condition relative to a large fixed λ with uniform weights.

Building on Theorem 1, we have the following overall convergence guarantee after the warm-up phase.

Theorem 2 (ε -stationarity after warm-up). *Suppose Assumptions 1 to 6 hold and that $\lambda_t \equiv \lambda$ and $L_t \leq L_{\text{max}}$ for all $t \geq T_{\text{warm}}$. We consider T communication rounds after T_{warm} ; for notational convenience, we re-index these rounds as $t \in \{1, \dots, T\}$. Each round has S local steps, so there are $K := TS$ total local updates in this phase. For any client i , the iterates of FedAPA satisfy*

$$\begin{aligned} \frac{1}{K} \sum_{t=1}^T \sum_{s=0}^{S-1} \mathbb{E}[\|\nabla \mathcal{L}_{i,t}(w_{i,t,s})\|^2] &\leq \frac{2\Delta_i}{K\eta} + L_{\text{max}} \eta \sigma^2 \\ &\quad + 2\lambda \Gamma(\tau) k_{\text{glob}} G, \end{aligned} \quad (27)$$

for any stepsize $0 < \eta \leq 1/L_{\text{max}}$, where

$$\Delta_i := \mathbb{E}[\mathcal{L}_{i,T_{\text{warm}}}(w_{i,T_{\text{warm}},0})] - L_{\text{inf}}. \quad (28)$$

Moreover, for any target $\varepsilon > 0$, if the parameters satisfy

$$0 < \eta \leq \min \left\{ \frac{1}{L_{\text{max}}}, \frac{\varepsilon}{3L_{\text{max}} \sigma^2} \right\}, \quad (29)$$

$$\lambda \leq \frac{\varepsilon}{6\Gamma(\tau) k_{\text{glob}} G}, \quad (30)$$

$$T \geq \frac{6\Delta_i}{\varepsilon \eta S}, \quad (31)$$

then FedAPA achieves ε -stationarity for client i :

$$\frac{1}{K} \sum_{t=1}^T \sum_{s=0}^{S-1} \mathbb{E}[\|\nabla \mathcal{L}_{i,t}(w_{i,t,s})\|^2] \leq \varepsilon. \quad (32)$$

Theorem 2 shows that, after warm-up, $\lambda_t \equiv \lambda$, the time-averaged gradient norm for any client is bounded by an initial gap term $O(1/(K\eta))$, a variance term $O(\eta)$, and a prototype-coupling term proportional to $\lambda \Gamma(\tau) k_{\text{glob}} G$. For any target $\varepsilon > 0$, the theorem gives explicit conditions on η, λ, τ and the number of rounds T ensuring this bound is at most ε ; the asymptotic error floor is of order $\lambda \Gamma(\tau) k_{\text{glob}} G$, so larger $\Gamma(\tau)$ or k_{glob} require smaller λ . The influence of similarity-weighted prototypes and warm-up is fully captured by the constants $\Gamma(\tau)$, k_{glob} , and λ ; in practice, smaller τ tends to increase $\Gamma(\tau)$ and thus tighten the admissible range of λ , while moderate τ can mitigate this effect. With standard stepsize choices (e.g., η on the order of ε or $1/\sqrt{K}$), the bound recovers the usual $O(1/\sqrt{K})$ rate for nonconvex stochastic methods, up to constants from prototype coupling. We refer the reader to Appendix A for detailed proofs.

VI. EXPERIMENTAL EVALUATION

In this section, we evaluate our proposed FedAPA method using a real-world distributed Wi-Fi CSI people-counting dataset collected across six distinct scenarios, including living

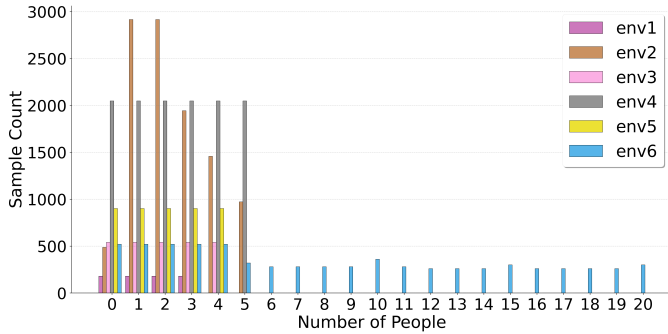


Fig. 4. Data distribution of six distinct environments.

TABLE II

ARCHITECTURE OVERVIEW AND LAYER CONFIGURATIONS FOR TINYCONVNET4, MIDDLECONVNET4, AND LARGECONVNET4 MODELS. ALL CONVOLUTIONAL LAYERS USE 3×3 KERNELS WITH STRIDE 2 UNLESS OTHERWISE SPECIFIED. 'C' DENOTES THE NUMBER OF OUTPUT CHANNELS.

Layer Information		Model Configurations		
Layer Block	Layer Type	TinyConvNet4 (C / Shape)	MiddleConvNet4 (C / Shape)	LargeConvNet4 (C / Shape)
Block 1	Conv2d	256 / (500, 121)	16 / (500, 121)	16 / (500, 121)
	BatchNorm2d	256	16	16
	ReLU	-	-	-
Block 2	Conv2d	-	32 / (250, 61)	32 / (250, 61)
	BatchNorm2d	-	32	32
	ReLU	-	-	-
Block 3	Conv2d	-	-	64 / (125, 31)
	BatchNorm2d	-	-	64
	ReLU	-	-	-
Block 4	Conv2d	-	-	128 / (63, 16)
	BatchNorm2d	-	-	128
	ReLU	-	-	-
Block 5	Conv2d	-	-	256 / (32, 8)
	BatchNorm2d	-	-	256
	ReLU	-	-	-
Pooling	AdaptiveAvgPool2d	(256, 1, 1)	(32, 1, 1)	(256, 1, 1)
Head	Conv2d ($1 \times 1, s = 1$)	-	256 / (1, 1)	256 / (1, 1)
Classifier	Linear	20	20	20
Total Params	-	7.96 K	18.44 K	463.75 K
FLOPs (MFLOPs)	-	340.75	162.85	606.35

Note: '-' indicates the layer/block is not present in that model variant.

room, classroom, bus, conference room, and hotel room. We first introduce the dataset and model architectures used in our experiments. Then, we present the implementation details, including hyperparameter settings and evaluation metrics. Finally, we compare our method with several FL methods and conduct extensive ablation studies to validate the effectiveness of each component in our proposed framework.

A. Datasets and Models

Fig. 4 shows the heterogeneous data distribution across six distinct environments, ranging between 0 and 20 people. Two of the six distinct environments for collecting CSI-based crowd counting data: a living room and a conference room, are depicted in Figs. 1 (a) and (b). To simulate model heterogeneity in the Wi-Fi CSI-based crowd counting task where resource constraints exist, we design three CNN architectures and assign them based on the training data of each client. Table II presents the number of layers, parameters, and computational costs for each model. By default, we use LargeConvNet4 in the subsequent experiments, except in the model heterogeneity setting experiments.

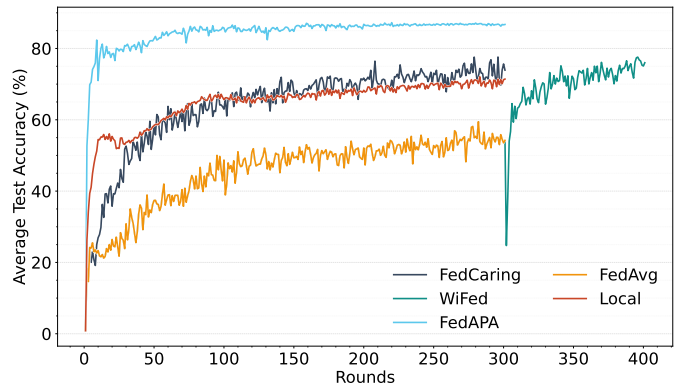


Fig. 5. The convergence behavior of different methods in heterogeneous data.

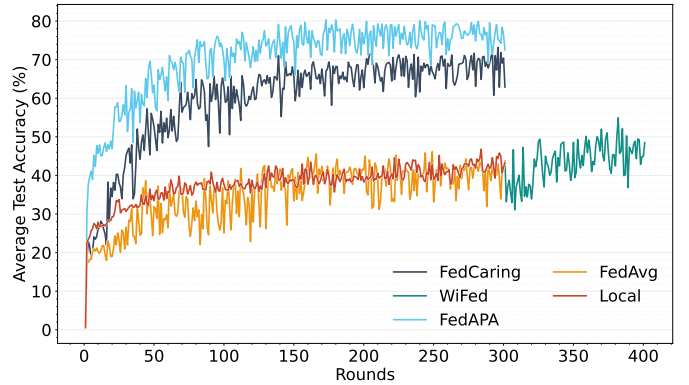


Fig. 6. The convergence behavior of different methods in heterogeneous model.

B. Data Preprocessing

We first filter out null subcarriers as they introduce outliers and degrade learning performance [2]. Then a sliding window with a size of 1,000 without overlapping is applied to segment the CSI data along the time axis. Each segment is then transformed into a $1,000 \times 242$ matrix, where 1,000 represents the number of CSI samples and 242 represents the number of subcarriers.

C. Baselines

We compare our method with local training and various FL methods that applied in Wi-Fi sensing tasks. Among them, WiFederated [28] fine-tuned the global model trained based on FedAvg [21] to build personalized models for each client. CARING [27] proposed a weight adaptation scheme that automatically assigns two different weights (i.e., 0.3 and 1) to each local model during model aggregation.

D. Implementation Details

The client participation ratio ρ controls the fraction of clients sampled each round. When the number of clients is large, a smaller ρ reduces bandwidth per round; in our setting with few clients, we use full participation and set $\rho = 1.0$. The number of local epochs E determines the interval between communication rounds; we set $E = 1$ for all experiments.

For local training we use stochastic gradient descent (SGD) with batch size 16, learning rate 10^{-2} , momentum 0.5, and

TABLE III
THE OVERALL PERFORMANCE COMPARISON OF DIFFERENT METHODS IN BOTH HETEROGENEOUS STATISTICAL DATA AND MODEL ARCHITECTURE SETTINGS.

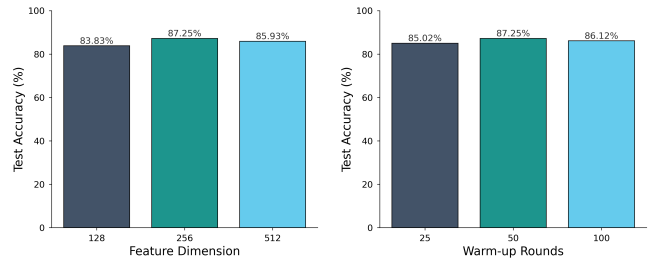
Heterogeneous Setting	Statistical Data			Model Architecture		
	Metric	Acc.	F1	MAE	Acc.	F1
Local	72.06	71.32	0.69	46.81	39.45	1.26
FedAvg [21]	59.46	38.26	2.01	46.16	37.51	2.03
WiFed [28]	<u>77.57</u>	<u>76.91</u>	<u>0.57</u>	54.94	47.80	1.34
FedCaring [27]	<u>77.60</u>	69.18	0.62	<u>70.00</u>	<u>68.43</u>	<u>0.77</u>
FedAPA	87.25	85.91	0.23	80.31	78.94	0.48

weight decay 10^{-5} . To reflect a personalized FL use case, evaluation is performed on each client’s local test split. We report Accuracy, F1, and mean absolute error (MAE); F1 is included to handle class imbalance [45]. To reduce variance, we average metrics over the last five communication rounds in all tables. FedAPA results are highlighted in **bold**, and the best results among those baselines are underlined. Each client uses a local split with 80% of data for training and 20% for testing. Experiments are run with PyTorch 2.7.1 on a server with two Intel Xeon Silver 4210R CPUs (20 cores), 128,GB RAM, and four NVIDIA RTX,3090 GPUs, running Ubuntu 24.04.

E. Performance Evaluation and Analysis

In this section, we compare FedAPA with multiple baselines, including traditional FL methods and FL methods that focus on statistical data. Hyperparameter settings of those baseline approaches are configured according to prior works [27], [28]. Extensive experiments were conducted to provide a comprehensive analysis of our methods.

1) *Practical heterogeneity setting*: The results of all algorithms in the practical heterogeneity setting are shown in Table III, and their convergence behavior is illustrated in Fig. 5 and Fig. 6. Here we use data and model heterogeneity settings to have a comprehensive evaluation of our methods in heterogeneous Wi-Fi CSI-based crowd counting tasks. Compared with other baselines, FedAPA is the top-performing method in both model heterogeneity and data heterogeneity setting. For the data heterogeneity setting, FedAPA increases the local accuracy, F1, and MAE by 15.19%, 14.59%, and 0.46 respectively. In the model heterogeneity setting, FedAPA increases the local accuracy, F1, and MAE by 33.5%, 39.49%, and 0.78 respectively. It is worth noting that the FedAPA method has worse sensing performance in the model heterogeneity setting. Those methods that include simple model parameter averaging also encounter performance degradation in the model heterogeneity scenario, which suggests a more sophisticated model aggregation mechanism during the global model generation. In this practical heterogeneity setting, the local data distributions and model architectures across all clients become imbalanced. Consequently, the F1 metrics of all algorithms are inferior to their accuracies. Moreover, simply averaging the model parameters may introduce significant local drift updates in heterogeneous model scenarios. FedAvg performs worse than the majority of other baselines. After



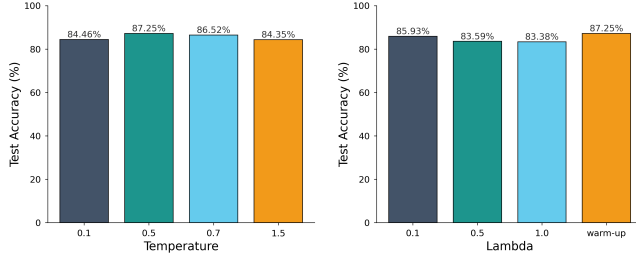
(a) Impact of feature dimensions (b) Impact of warm-up rounds

Fig. 7. Impact of (a) feature dimensions and (b) warm-up rounds on FedAPA performance.

fine-tuning over several epochs using either original or re-balanced local data, the performance is remarkably improved, as demonstrated by the WiFed. This suggests that fine-tuning from a pre-trained representation can help improve the Wi-Fi sensing performance under heterogeneous settings. FedAPA further outperforms WiFed in either data or model heterogeneity settings, even without fine-tuning from local data, which demonstrates its superior capability in tackling heterogeneous tasks. The performance of FedCaring also suggests that by carefully assigning weights to local models during aggregation, the negative impact of data and model heterogeneity can be alleviated. However, FedCaring still falls short of FedAPA, which indicates that simply assigning two different weights to local models is insufficient to capture the complex relationships among clients.

2) *Impact of different feature dimensions for embeddings*: As cosine score is used to measure the similarity between embeddings and prototypes, the feature dimension of embeddings may affect the performance of FedAPA. We conduct experiments with different feature dimensions, including 128, 256, and 512. The results are shown in Fig. 7a. It can be observed that the performance of FedAPA improves as the feature dimension increases from 128 to 256. However, when the feature dimension is further increased to 512, the performance slightly decreases. This suggests that a moderate feature dimension is beneficial for capturing the essential characteristics of the data while avoiding overfitting or redundancy in the embeddings. Therefore, we choose 256 as the default feature dimension for our experiments.

3) *Impact of different warm-up rounds*: Another important hyperparameter is the number of warm-up rounds T_{warm} , which controls the length of the representation learning warm-up phase. We conduct experiments with different warm-up rounds, including 25, 50, and 100. The results are shown in Fig. 7b. A similar trend can be observed that the performance of FedAPA improves as the number of warm-up rounds increases from 25 to 50. However, when the number of warm-up rounds is further increased to 100, the performance slightly decreases. This suggests that a moderate number of warm-up rounds is beneficial for stabilizing training and guiding the model through a logical progression of learning stages. Too short warm-up rounds may cause the contrastive loss to dominate the training process early, leading to suboptimal performance. Conversely, too long warm-up rounds may delay the influence



(a) Impact of different temperatures. (b) Impact of warm-up based λ coefficient.

Fig. 8. Impact of (a) different temperatures and (b) warm-up based λ coefficient on FedAPA performance.

of contrastive loss, hindering the model’s ability to learn robust representations. Therefore, we choose 50 as the default number of warm-up rounds for our experiments.

4) *Impact of different temperatures for contrastive loss terms and prototype aggregation:* Temperature τ is a crucial hyperparameter in cosine similarity to adjust the tolerance for feature distribution [46]. We conduct experiments with different temperatures, including 0.1, 0.5, 0.7, and 1.5. The results are shown in Fig. 8a. It can be observed that the performance of FedAPA improves as the temperature increases from 0.1 to 0.5. However, when the temperature is further increased from 0.5 to 1.5, the performance slightly decreases. This suggests that a moderate temperature is beneficial for balancing the influence of negatives and preventing over-smoothing or over-sharpening of the similarity scores. Therefore, we choose 0.5 as the default temperature for our experiments.

5) *The impact of the coefficient (λ) on representation learning:* λ is another importance hyperparameter that balances the contribution of contrastive representation learning and classification learning. We compare our warm-up based coefficient with three static coefficients, including 0.1, 0.5, and 1.0. The results are shown in Fig. 8b. As indicated by results, configurations with a static coefficient perform worse when compared to our warm-up based coefficient setting. The use of a static coefficient leads to the model encoder excessively focusing on either contrastive representation learning early (thereby compromising classification performance) or classification learning (thus hindering the development of globally informative representations). This suggests that by warming up the coefficient during a certain number of rounds, the model can gradually increase the emphasis on contrastive representation learning, leading to better overall performance. This adaptive approach results in enhanced performance of the model encoder and greater robustness.

6) *Impact of similarity-aware prototype aggregation and other clients’ prototypes involvement:* To validate the effectiveness of our proposed similarity-aware prototype aggregation method, we conduct experiments comparing it with a simple global average prototype aggregation method. In the global average prototype aggregation method, the server computes the global prototype for each class by averaging the prototypes from all clients without considering their similarities. The results are shown in Table IV. It can be observed that our proposed similarity-aware prototype aggregation method significantly

TABLE IV
THE EFFECT OF SIMILARITY-AWARE PROTOTYPE AGGREGATION AND OTHER CLIENTS’ PROTOTYPES INVOLVEMENT.

Heterogeneous Setting		Statistical Data			Model Architecture		
Metric		Acc.	F1	MAE	Acc.	F1	MAE
Global Avg. Proto		74.02	73.59	0.71	54.75	47.89	1.62
Global Avg. Proto with Client Protos		<u>82.03</u>	<u>81.47</u>	<u>0.38</u>	<u>69.41</u>	<u>67.20</u>	<u>0.77</u>
FedAPA		87.25	85.91	0.23	80.31	78.94	0.48

TABLE V
THE THEORETICAL AND PRACTICAL COMMUNICATION COST PER COMMUNICATION ROUND FOR EACH CLIENT USING LARGECONVNET4.

Methods	Theoretical	Practical
FedAvg [21]	$2 * \sum_w$	<u>3,710 KB</u>
FedCaring [27]	$2 * \sum_w$	<u>3,710 KB</u>
WiFederated [28]	$2 * \sum_w$	<u>3,710 KB</u>
FedAPA	$\sum_p * (\sum_{N+1} C)$	150.53 KB

outperforms the simple global average prototype aggregation method in both data and model heterogeneity settings. This suggests that by considering the similarities between clients’ prototypes, our method can effectively capture the relationships among clients and generate more informative global prototypes for each client. Additionally, we also evaluate the impact of involving other clients’ prototypes in the local contrastive loss. The results indicate that incorporating other clients’ prototypes further enhances the performance of our method, demonstrating the benefits of leveraging information from multiple clients to improve local representation learning.

7) *Communication overhead:* Apart from analyzing sensing performance, we also evaluate the communication cost per round for each client, which provides a comprehensive performance evaluation of our proposed framework. The communication overhead for each algorithm is assessed based on the callops [47] library. Table V presents the detailed overhead results, where \sum_w denotes the total number of parameters in a model, and \sum_p indicates the total number of parameters in a prototype. It shows that our FedAPA approach has the least communication overhead when compared with those model-sharing based approaches. Fine-tuning approaches based on FedAvg, which involve uploading and downloading full models to and from the PS, have similar (and much larger) overhead. In contrast, FedAPA only requires the exchange of global and local prototypes, resulting in significantly lower communication costs. This makes FedAPA more suitable for deployment in resource-constrained environments where communication bandwidth is limited.

VII. DISCUSSIONS

Applying FL to cross-domain Wi-Fi sensing involves trade-offs among label availability, communication, computation, and scalability; no single design can optimize all dimensions at once. We next discuss key limitations of our approach.

A. Scalability and Client Selection Strategy

Partial client participation better reflects real deployments, where many devices cannot connect to the PS in every round

[48]. Selecting only a subset of clients reduces uplink traffic but can degrade performance if the policy ignores representation diversity and system heterogeneity. While we do not evaluate FedAPA under partial participation, we suggest that a client selection strategy considering prototype diversity and device capability could enhance efficiency without compromising accuracy. In short, partial participation saves bandwidth, but selection must preserve informative clients while limiting overhead.

B. Label Scarcity

Our methods assume supervised learning. In practice, labeled CSI is scarce: ordinary users rarely annotate data and labels are expensive to curate in cross-domain Wi-Fi scenarios. This gap suggests moving from purely supervised FL toward semi-supervised or unsupervised formulations that exploit large volumes of unlabeled, crowdsourced CSI while preserving privacy.

C. Computation Efficiency and Communication Cost

Computation and communication jointly determine the practicality of FL systems. FedAPA communicates only global and local prototypes, which lowers communication overhead compared with approaches that exchange full model parameters. However, the additional prototype-based loss in the local training loop increases on-device computation, so there is a trade-off between reduced communication overhead and extra local compute.

VIII. CONCLUSION

This paper addresses statistical and model heterogeneity in distributed Wi-Fi CSI-based crowd counting with FedAPA, a federated learning method built around an adaptive prototype aggregation module. APA performs similarity-weighted aggregation of class prototypes, so clients with related distributions exchange compact class-level representations instead of full models, improving collaboration while preserving personalization and reducing communication overhead. Each local model is decomposed into an encoder and a classifier to enable shared representation learning with personalized decision layers. To align local and global knowledge, we adopt a hybrid local objective that couples classification loss with a prototype-contrastive loss under a warm-up schedule. We further provide a non-convex convergence analysis under standard smoothness and bounded-variance conditions to provide theoretical insight. Experiments on a Wi-Fi CSI crowd-counting dataset with six environments show consistent gains over FL-based Wi-Fi sensing baselines and substantially lower client-side bandwidth. This study focuses on a single sensing task; future work will extend FedAPA to multi-task settings for cross-task collaboration, move toward a Wi-Fi sensing foundation model with low communication cost, and investigate test-time environmental dynamics with unsupervised domain adaptation in the FL pipeline.

REFERENCES

- [1] J. Guo, I. W.-H. Ho, Y. Hou, and Z. Li, "Fedpos: A federated transfer learning framework for csi-based wi-fi indoor positioning," *IEEE Systems Journal*, 2023.
- [2] J. Guo, W. Zhuang, Y. Mao, and I. W.-H. Ho, "Rssi-assisted csi-based passenger counting with multiple wi-fi receivers," *2025 IEEE Wireless Communications and Networking Conference (WCNC)*, pp. 1–6, 2025.
- [3] S. T. Kouyoumdjieva, P. Danielis, and G. Karlsson, "Survey of non-image-based approaches for counting people," *IEEE Communications Surveys & Tutorials*, vol. 22, no. 2, pp. 1305–1336, 2019.
- [4] J. Weppner and P. Lukowicz, "Bluetooth based collaborative crowd density estimation with mobile phones," *2013 IEEE international conference on pervasive computing and communications (PerCom)*, pp. 193–200, 2013.
- [5] G. Gao, J. Gao, Q. Liu, Q. Wang, and Y. Wang, "Cnn-based density estimation and crowd counting: A survey," *arXiv preprint arXiv:2003.12783*, 2020.
- [6] J. Xiao, H. Li, M. Wu, H. Jin, M. J. Deen, and J. Cao, "A survey on wireless device-free human sensing: Application scenarios, current solutions, and open issues," *ACM Computing Surveys*, vol. 55, no. 5, pp. 1–35, 2022.
- [7] Y. He, Y. Chen, Y. Hu, and B. Zeng, "WiFi vision: Sensing, recognition, and detection with commodity mimo-ofdm wifi," *IEEE Internet of Things Journal*, vol. 7, no. 9, pp. 8296–8317, 2020.
- [8] S. Depatla, A. Muralidharan, and Y. Mostofi, "Occupancy estimation using only wifi power measurements," *IEEE Journal on Selected Areas in Communications*, vol. 33, no. 7, pp. 1381–1393, 2015.
- [9] Z. Yang, Z. Zhou, and Y. Liu, "From rssi to csi: Indoor localization via channel response," *ACM Computing Surveys (CSUR)*, vol. 46, no. 2, pp. 1–32, 2013.
- [10] J. Liu, H. Liu, Y. Chen, Y. Wang, and C. Wang, "Wireless sensing for human activity: A survey," *IEEE Communications Surveys & Tutorials*, vol. 22, no. 3, pp. 1629–1645, 2019.
- [11] H. Wang, Y. Ge, and I. W.-H. Ho, "Wall-proximity matters: Understanding the effect of device placement with respect to the wall for indoor wi-fi sensing," *arXiv preprint arXiv:2412.13208*, 2024.
- [12] Y. Zhao, S. Liu, F. Xue, B. Chen, and X. Chen, "Deepcount: Crowd counting with wi-fi using deep learning," *Journal of Communications and Information Networks*, vol. 4, no. 3, pp. 38–52, 2019.
- [13] H. Jiang, S. Chen, Z. Xiao, J. Hu, J. Liu, and S. Dustdar, "Pa-count: Passenger counting in vehicles using wi-fi signals," *IEEE Transactions on Mobile Computing*, 2023.
- [14] J. Guo and I. W.-H. Ho, "Csi-based efficient self-quarantine monitoring system using branchy convolution neural network," *2022 IEEE 8th World Forum on Internet of Things*, pp. 1–6, 2022.
- [15] H. Wang, J. Guo, and I. W.-H. Ho, "Guiding wi-fi sensor placement for enhanced csi-based sensing in stationary crowd counting," *IEEE Internet of Things Journal*, 2025.
- [16] S. Tan, Y. Ren, J. Yang, and Y. Chen, "Commodity wifi sensing in ten years: Status, challenges, and opportunities," *IEEE Internet of Things Journal*, vol. 9, no. 18, pp. 17 832–17 843, 2022.
- [17] J. Liu, Y. He, C. Xiao, J. Han, and K. Ren, "Time to think the security of wifi-based behavior recognition systems," *IEEE Transactions on Dependable and Secure Computing*, 2023.
- [18] Q. Yang, Y. Liu, T. Chen, and Y. Tong, "Federated machine learning: Concept and applications," *ACM Transactions on Intelligent Systems and Technology*, vol. 10, no. 2, pp. 1–19, Mar. 2019.
- [19] A. Z. Tan, H. Yu, L. Cui, and Q. Yang, "Towards personalized federated learning," *IEEE Transactions on Neural Networks and Learning Systems*, 2022.
- [20] D. Gao, X. Yao, and Q. Yang, "A survey on heterogeneous federated learning," *arXiv preprint arXiv:2210.04505*, 2022.
- [21] B. McMahan, E. Moore, D. Ramage, S. Hampson, and B. A. y Arcas, "Communication-efficient learning of deep networks from decentralized data," *Artificial intelligence and statistics*, pp. 1273–1282, 2017.
- [22] Q. Li, B. He, and D. Song, "Model-contrastive federated learning," *Proceedings of the IEEE/CVF Conference on Computer Vision and Pattern Recognition*, pp. 10 713–10 722, 2021.
- [23] Y. Tan, G. Long, L. Liu, T. Zhou, Q. Lu, J. Jiang, and C. Zhang, "FedProto: Federated prototype learning across heterogeneous clients," *Proceedings of the AAAI Conference on Artificial Intelligence*, vol. 36, no. 8, pp. 8432–8440, 2022.
- [24] Q. Li, Y. Diao, Q. Chen, and B. He, "Federated learning on non-iid data silos: An experimental study," *2022 IEEE 38th International Conference on Data Engineering (ICDE)*, pp. 965–978, 2022.

- [25] H. Zou, Y. Zhou, J. Yang, W. Gu, L. Xie, and C. Spanos, "Freecount: Device-free crowd counting with commodity wifi," in *GLOBECOM 2017-2017 IEEE Global Communications Conference*. IEEE, 2017, pp. 1–6.
- [26] H. Hou, S. Bi, L. Zheng, X. Lin, Y. Wu, and Z. Quan, "Dasecount: Domain-agnostic sample-efficient wireless indoor crowd counting via few-shot learning," *IEEE Internet of Things Journal*, vol. 10, no. 8, pp. 7038–7050, 2022.
- [27] X. Li, F. Song, M. Luo, K. Li, L. Chang, X. Chen, and Z. Wang, "Caring: Towards collaborative and cross-domain wi-fi sensing," *IEEE Transactions on Mobile Computing*, 2023.
- [28] S. M. Hernandez and E. Bulut, "WiFederated: Scalable wifi sensing using edge-based federated learning," *IEEE Internet of Things Journal*, vol. 9, no. 14, pp. 12628–12640, 2021.
- [29] K. Zhang, X. Liu, X. Xie, J. Zhang, B. Niu, and K. Li, "A cross-domain federated learning framework for wireless human sensing," *IEEE Network*, vol. 36, no. 5, pp. 122–128, 2022.
- [30] P. Liu, G. Zhu, W. Jiang, W. Luo, J. Xu, and S. Cui, "Vertical federated edge learning with distributed integrated sensing and communication," *IEEE Communications Letters*, vol. 26, no. 9, pp. 2091–2095, 2022.
- [31] L. Collins, H. Hassani, A. Mokhtari, and S. Shakkottai, "Exploiting shared representations for personalized federated learning," *International Conference on Machine Learning*, pp. 2089–2099, 2021.
- [32] X. Li, M. JIANG, X. Zhang, M. Kamp, and Q. Dou, "Fedbn: Federated learning on non-iid features via local batch normalization," *International Conference on Learning Representations*, 2021.
- [33] J. Zhang, Y. Hua, H. Wang, T. Song, Z. Xue, R. Ma, and H. Guan, "FedALA: Adaptive local aggregation for personalized federated learning," *Proceedings of the AAAI Conference on Artificial Intelligence*, vol. 37, no. 9, pp. 11 237–11 244, 2023.
- [34] Y. Huang, L. Chu, Z. Zhou, L. Wang, J. Liu, J. Pei, and Y. Zhang, "Personalized cross-silo federated learning on non-iid data," *Proceedings of the AAAI Conference on Artificial Intelligence*, vol. 35, no. 9, pp. 7865–7873, 2021.
- [35] F. Gringoli, M. Schulz, J. Link, and M. Hollick, "Free your CSI: A channel state information extraction platform for modern Wi-Fi chipsets," *WiNTECH '19: Proceedings of the 13th International Workshop on Wireless Network Testbeds, Experimental Evaluation & Characterization*, 2019.
- [36] J. Snell, K. Swersky, and R. Zemel, "Prototypical networks for few-shot learning," *Advances in neural information processing systems*, vol. 30, 2017.
- [37] Y. Tan, G. Long, J. Ma, L. Liu, T. Zhou, and J. Jiang, "Federated learning from pre-trained models: A contrastive learning approach," *Advances in neural information processing systems*, vol. 35, pp. 19 332–19 344, 2022.
- [38] X. Mu, Y. Shen, K. Cheng, X. Geng, J. Fu, T. Zhang, and Z. Zhang, "FedProc: Prototypical contrastive federated learning on non-iid data," *Future Generation Computer Systems*, vol. 143, pp. 93–104, 2023.
- [39] H. V. Nguyen and L. Bai, "Cosine similarity metric learning for face verification," *Asian conference on computer vision*, pp. 709–720, 2010.
- [40] R. Ye, Z. Ni, F. Wu, S. Chen, and Y. Wang, "Personalized federated learning with inferred collaboration graphs," *International conference on machine learning*, pp. 39 801–39 817, 2023.
- [41] Y. Bengio, J. Louradour, R. Collobert, and J. Weston, "Curriculum learning," in *Proceedings of the 26th annual international conference on machine learning*, 2009, pp. 41–48.
- [42] S. Ghadimi and G. Lan, "Stochastic first-and zeroth-order methods for nonconvex stochastic programming," *SIAM journal on optimization*, vol. 23, no. 4, pp. 2341–2368, 2013.
- [43] S. Lee, J. Park, and J. Lee, "Implicit jacobian regularization weighted with impurity of probability output," *International Conference on Machine Learning*, pp. 19 141–19 184, 2023.
- [44] L. Newhouse, "Softmax is 1/2-lipschitz (in a norm that may not matter)," 2025. [Online]. Available: <https://www.lakernewhouse.com/assets/writing/softmax-is-0-5-lipschitz.pdf>
- [45] H. He and E. A. Garcia, "Learning from imbalanced data," *IEEE Transactions on Knowledge and Data Engineering*, vol. 21, no. 9, pp. 1263–1284, 2009.
- [46] T. Chen, S. Kornblith, M. Norouzi, and G. Hinton, "A simple framework for contrastive learning of visual representations," in *International conference on machine learning*. PMLR, 2020, pp. 1597–1607.
- [47] callops: a FLOPs and Params calculate tool for neural networks, 2023, <https://github.com/MrYxJ/calculate-flops.pytorch> [Accessed 02 Dec. 2023].
- [48] Y. J. Cho, J. Wang, and G. Joshi, "Client selection in federated learning: Convergence analysis and power-of-choice selection strategies," *arXiv preprint arXiv:2010.01243*, 2020.

APPENDIX A CONVERGENCE ANALYSIS

This appendix contains the full convergence analysis for FedAPA. It includes all notations, detailed assumptions, and complete proofs of lemmas and theorems in the main article.

A. Notations

Communication rounds are $t \in \{1, \dots, T\}$, local steps are $s \in \{0, \dots, S-1\}$, and $K := TS$. Clients are $i \in \{1, \dots, N\}$. Client i has an encoder $f_i(\cdot; w_{i,t}^\theta)$ and a classifier $w_{i,t}^h$ at round t ; write $w_{i,t} = (w_{i,t}^\theta, w_{i,t}^h)$. The stochastic gradient at local step (t, s) is $g_{i,t,s}$. Write $\mathbf{Q}_{i,t} := \{\mathbf{q}_{i,t}^c\}_{c \in \mathcal{C}}$ and $\mathbf{Q}_t := \mathbf{Q}_\tau(\mathbf{P}_t) := \{\mathbf{Q}_{i,t}\}_{i=1}^N$. Within round t , with \mathbf{P}_t and \mathbf{Q}_t fixed, client i optimizes the local objective

$$\mathcal{L}_{i,t}(w) := \mathcal{L}_{\text{ce},i}(w) + \lambda_t \Phi_i(w; \mathbf{Q}_{t-1}, \mathbf{P}_{t-1}), \quad t \geq 1, \quad (33)$$

where \mathcal{L}_{ce} is the cross-entropy loss and Φ_i collects the prototype-based contrastive terms $\mathcal{L}_g + \mathcal{L}_c$ defined in Section IV-C. For $t = 1$, we assume an randomly initialized prototype set $(\mathbf{P}_0, \mathbf{Q}_0)$. At t -th round, clients update prototypes to \mathbf{P}_t and the server constructs $\mathbf{Q}_t = \mathbf{Q}_\tau(\mathbf{P}_t)$, which are then used in the next round via (33). The schedule $\{\lambda_t\}$ follows the cosine warm-up in Section IV-C, and becomes constant after T_{warm} rounds. For convenience define the per-round stationarity metric

$$G_{i,t}^2 := \sum_{s=0}^{S-1} \mathbb{E}[\|\nabla \mathcal{L}_{i,t}(w_{i,t,s})\|^2]. \quad (34)$$

B. Assumptions

We assume full participation. Let $L_{\text{inf}} \in \mathbb{R}$ denote a uniform lower bound of all considered objectives. The following conditions are used in the analysis.

Assumption 1 (Smoothness and lower boundedness). *The cross-entropy term $\mathcal{L}_{\text{ce},i}$ is L_{ce} -smooth, and the regularizer $\Phi_i(\cdot; \mathbf{Q}, \mathbf{P})$ is L_Φ -smooth in w , uniformly in (\mathbf{Q}, \mathbf{P}) . Fix round t and the prototype stacks \mathbf{P}_{t-1} and $\mathbf{Q}_\tau(\mathbf{P}_{t-1})$. Then the per-round objective $\mathcal{L}_{i,t}$ defined in (33) is L_t -smooth:*

$$\|\nabla \mathcal{L}_{i,t}(u) - \nabla \mathcal{L}_{i,t}(v)\| \leq L_t \|u - v\|, \quad \forall u, v, \quad (35)$$

with $L_t = L_{\text{ce}} + \lambda_t L_\Phi$, and after warm-up $L_t \leq L_{\text{max}} := L_{\text{ce}} + \lambda L_\Phi$. There also exists L_{inf} such that

$$\mathcal{L}_{i,t}(w) \geq L_{\text{inf}} \quad \forall i, t, w. \quad (36)$$

Assumption 2 (Stochastic gradient regularity). *At local step (i, t, s) , the stochastic gradient $g_{i,t,s}$ is an unbiased estimate of the true gradient with bounded variance:*

$$\mathbb{E}[g_{i,t,s} \mid w_{i,t,s}] = \nabla \mathcal{L}_{i,t}(w_{i,t,s}), \quad (37)$$

$$\mathbb{E}[\|g_{i,t,s} - \nabla \mathcal{L}_{i,t}(w_{i,t,s})\|^2] \leq \sigma^2, \quad (38)$$

for some $\sigma^2 \geq 0$, uniformly over all i, t, s . Moreover, there exists a global constant $G > 0$ such that

$$\mathbb{E}[\|g_{i,t,s}\|^2] \leq G^2 \quad \text{for all } i, t, s. \quad (39)$$

Under Assumption 3, bounded encoder outputs and prototypes (including padded ones) ensure that the gradients of the

cross-entropy and prototype-based contrastive losses remain uniformly bounded, so such G exists.

Assumption 3 (Bounded and Lipschitz representations). *The encoder output is uniformly bounded: $\|\mathbf{r}_{w^\theta}(\mathbf{h})\| \leq 1$ for all w^θ, \mathbf{h} . Each prototype $\mathbf{p}_{i,t}^c$ is an empirical mean of such embeddings, so $\|\mathbf{p}_{i,t}^c\| \leq 1$. The same bound holds for padded prototypes introduced in Section IV-B of main article, since they are averages of existing bounded prototypes. Moreover, the encoder is Lipschitz in its parameters: there exists $L_{w^\theta} > 0$ such that*

$$\|\mathbf{r}_{w^\theta}(\mathbf{h}) - \mathbf{r}_{\hat{w}^\theta}(\mathbf{h})\| \leq L_{w^\theta} \|w^\theta - \hat{w}^\theta\|, \quad \forall w^\theta, \hat{w}^\theta, \mathbf{h}. \quad (40)$$

Assumption 4 (Lipschitz personalized aggregation). *Let \mathbf{P} denote the stacked local prototypes and define $\mathbf{Q}_\tau(\mathbf{P})$ via the similarity-weighted aggregation rule in Section IV-B. We assume that $\mathbf{Q}_\tau(\cdot)$ is Lipschitz with respect to \mathbf{P} : there exists a constant $L_{\text{agg}}(\tau) > 0$ such that*

$$\|\mathbf{Q}_\tau(\mathbf{P}) - \mathbf{Q}_\tau(\mathbf{P}')\|_F \leq L_{\text{agg}}(\tau) \|\mathbf{P} - \mathbf{P}'\|_F \quad \forall \mathbf{P}, \mathbf{P}'. \quad (41)$$

Under Assumption 3, all prototypes (including padded ones) have unit-norm bounds, and the softmax map with inverse temperature $1/\tau$ has Jacobian spectral norm $O(1/\tau)$. Hence $L_{\text{agg}}(\tau)$ can be chosen on the order of \sqrt{N}/τ . For example,

$$L_{\text{agg}}(\tau) \leq \frac{\sqrt{N}}{2\tau}. \quad (42)$$

Assumption 5 (Prototype-loss regularity). *For each client i , the prototype-based regularizer $\Phi_i(w; \mathbf{Q}, \mathbf{P})$ is Lipschitz in (\mathbf{Q}, \mathbf{P}) and uniformly bounded:*

(A5.1) *There exists $c_\Phi(\tau) > 0$ such that*

$$|\Phi_i(w; \mathbf{Q}, \mathbf{P}) - \Phi_i(w; \mathbf{Q}', \mathbf{P}')| \leq c_\Phi(\tau) \left(\|\mathbf{Q} - \mathbf{Q}'\|_F + \|\mathbf{P} - \mathbf{P}'\|_F \right), \quad (43)$$

(A5.2) *There exists $B_\Phi > 0$ such that $0 \leq \Phi_i(w; \mathbf{Q}, \mathbf{P}) \leq B_\Phi$ for all $w, \mathbf{Q}, \mathbf{P}$.*

These properties hold for both original and padded prototypes. Because the padded variants average unit-norm embeddings, they stay within the same bounded subset of the feature space.

Assumption 6 (Warm-up schedule). *The warm-up weight $\{\lambda_t\}_{t \geq 1}$ is nondecreasing and there exist $T_{\text{warm}} < \infty$ and $\lambda \geq 0$ such that*

$$\lambda_t = \lambda \quad \text{for all } t \geq T_{\text{warm}}. \quad (44)$$

C. Convergence results

Based on the above assumptions, we have the following convergence result for FedAPA:

We first state the standard descent result for one client with fixed prototypes.

Lemma 1 (One-step descent with fixed prototypes). *Let Assumptions 1 and 2 hold. Fix round t and client i , and suppose $\mathbf{P}_t, \mathbf{Q}_t, \lambda_t$ are fixed during the round. For step size*

$0 < \eta \leq 1/L_t$, the SGD update $w_{i,t,s+1} = w_{i,t,s} - \eta g_{i,t,s}$ satisfies

$$\begin{aligned} \mathbb{E}[\mathcal{L}_{i,t}(w_{i,t,s+1})] &\leq \mathbb{E}[\mathcal{L}_{i,t}(w_{i,t,s})] \\ &\quad - \eta \left(1 - \frac{L_t \eta}{2}\right) \mathbb{E}[\|\nabla \mathcal{L}_{i,t}(w_{i,t,s})\|^2] \\ &\quad + \frac{L_t \eta^2}{2} \sigma^2. \end{aligned} \quad (45)$$

Proof. During round t , prototypes are fixed. by Assumption 1, $\mathcal{L}_{i,t}$ is L_t -smooth. Let the SGD update be $w_{i,t,s+1} = w_{i,t,s} - \eta g_{i,t,s}$. By the standard smoothness inequality,

$$\begin{aligned} \mathcal{L}_{i,t}(w_{i,t,s+1}) &\leq \mathcal{L}_{i,t}(w_{i,t,s}) - \eta \langle \nabla \mathcal{L}_{i,t}(w_{i,t,s}), g_{i,t,s} \rangle \\ &\quad + \frac{L_{i,t} \eta^2}{2} \|g_{i,t,s}\|^2. \end{aligned} \quad (46)$$

Taking conditional expectation given $w_{i,t,s}$ and using Assumption 3,

$$\mathbb{E}[\langle \nabla \mathcal{L}_{i,t}(w_{i,t,s}), g_{i,t,s} \rangle \mid w_{i,t,s}] = \|\nabla \mathcal{L}_{i,t}(w_{i,t,s})\|^2, \quad (47)$$

$$\mathbb{E}[\|g_{i,t,s}\|^2 \mid w_{i,t,s}] \leq \|\nabla \mathcal{L}_{i,t}(w_{i,t,s})\|^2 + \sigma^2. \quad (48)$$

Plug these into (46) and then take total expectation to obtain

$$\begin{aligned} \mathbb{E}[\mathcal{L}_{i,t}(w_{i,t,s+1})] &\leq \mathbb{E}[\mathcal{L}_{i,t}(w_{i,t,s})] \\ &\quad - \eta \left(1 - \frac{L_t \eta}{2}\right) \mathbb{E}[\|\nabla \mathcal{L}_{i,t}(w_{i,t,s})\|^2] \\ &\quad + \frac{L_t \eta^2}{2} \sigma^2. \end{aligned} \quad (49)$$

which is (45). \square

Corollary 1 (S -step descent within a round). *Under the conditions of Lemma 1 and $\eta \leq 1/L_t$,*

$$\mathbb{E}[\mathcal{L}_{i,t}(w_{i,t,S})] \leq \mathbb{E}[\mathcal{L}_{i,t}(w_{i,t,0})] - \frac{\eta}{2} G_{i,t}^2 + \frac{L_t \eta^2}{2} S \sigma^2. \quad (50)$$

We next control how much prototypes move between rounds and how this affects the loss.

Lemma 2 (Prototype movement). *Suppose Assumptions 2 and 3 hold. Let $C_i := |C_i|$ be the number of classes at client i and $C_{\max} := \max_i C_i$. Let*

$$\|\Delta \mathbf{P}_t\|_F^2 = \sum_{i=1}^N \|\mathbf{P}_{i,t} - \mathbf{P}_{i,t-1}\|_F^2, \quad (51)$$

then

(a) Per-client movement. *For any client i and any round t ,*

$$\mathbb{E}[\|\Delta \mathbf{P}_t\|_F] \leq k_{\max} \eta S G, \quad (52)$$

where

$$k_i := L_{w^\theta} \sqrt{C_i}, \quad k_{\max} := L_{w^\theta} \sqrt{C_{\max}}, \quad (53)$$

and hence $k_i \leq k_{\max}$ for all i .

(b) Global movement. *Consequently, the stacked prototype matrix $\mathbf{P}_t := \{\mathbf{P}_{i,t}\}_{i=1}^N$ satisfies*

$$\mathbb{E}[\|\Delta \mathbf{P}_t\|_F] \leq k_{\text{glob}} \eta S G, \quad (54)$$

where

$$k_{\text{glob}} := L_{w^\theta} \sqrt{\sum_{i=1}^N C_i} \leq L_{w^\theta} \sqrt{N C_{\max}}. \quad (55)$$

Proof. Fix a client i and a class $c \in \mathcal{C}_i$. By definition,

$$\begin{aligned} \mathbf{p}_{i,t-1}^c &= \frac{1}{m_i^c} \sum_{\mathbf{h} \in \mathcal{D}_i^c} \mathbf{r}_{w_{i,t-1,S}^\theta}(\mathbf{h}), \\ \mathbf{p}_{i,t}^c &= \frac{1}{m_i^c} \sum_{\mathbf{h} \in \mathcal{D}_i^c} \mathbf{r}_{w_{i,t,S}^\theta}(\mathbf{h}), \end{aligned} \quad (56)$$

By Assumption 3,

$$\|\mathbf{r}_{w_{i,t,S}^\theta}(\mathbf{h}) - \mathbf{r}_{w_{i,t-1,S}^\theta}(\mathbf{h})\| \leq L_{w^\theta} \|\Delta w_{i,t}^\theta\| \quad \forall \mathbf{h} \in \mathcal{D}_i^c. \quad (57)$$

Hence

$$\begin{aligned} \|\mathbf{p}_{i,t}^c - \mathbf{p}_{i,t-1}^c\| &= \left\| \frac{1}{m_i^c} \sum_{\mathbf{h} \in \mathcal{D}_i^c} (\mathbf{r}_{w_{i,t,S}^\theta}(\mathbf{h}) - \mathbf{r}_{w_{i,t-1,S}^\theta}(\mathbf{h})) \right\| \\ &\leq \frac{1}{m_i^c} \sum_{\mathbf{h} \in \mathcal{D}_i^c} \|\mathbf{r}_{w_{i,t,S}^\theta}(\mathbf{h}) - \mathbf{r}_{w_{i,t-1,S}^\theta}(\mathbf{h})\| \\ &\leq \frac{1}{m_i^c} \sum_{\mathbf{h} \in \mathcal{D}_i^c} L_{w^\theta} \|\Delta w_{i,t}^\theta\| \\ &= L_{w^\theta} \|\Delta w_{i,t}^\theta\|. \end{aligned} \quad (58)$$

Therefore,

$$\|\mathbf{p}_{i,t}^c - \mathbf{p}_{i,t-1}^c\|^2 \leq L_{w^\theta}^2 \|\Delta w_{i,t}^\theta\|^2. \quad (59)$$

The encoder parameters follow the SGD recursion

$$w_{i,t,s+1}^\theta = w_{i,t,s}^\theta - \eta g_{i,t,s}^\theta, \quad (60)$$

where $s = 0, \dots, S-1$, so

$$\Delta w_{i,t}^\theta = w_{i,t,S}^\theta - w_{i,t,0}^\theta = -\eta \sum_{s=0}^{S-1} g_{i,t,s}^\theta. \quad (61)$$

Then

$$\begin{aligned} \|\Delta w_{i,t}^\theta\|^2 &= \eta^2 \left\| \sum_{s=0}^{S-1} g_{i,t,s}^\theta \right\|^2 \\ &\leq \eta^2 S \sum_{s=0}^{S-1} \|g_{i,t,s}^\theta\|^2 \\ &\leq \eta^2 S \sum_{s=0}^{S-1} \|g_{i,t,s}\|^2, \end{aligned} \quad (62)$$

where we used $\|g_{i,t,s}^\theta\| \leq \|g_{i,t,s}\|$ and the Cauchy-Schwarz inequality. Taking expectations and using Assumption 2 ($\mathbb{E}\|g_{i,t,s}\|^2 \leq G^2$) yields

$$\mathbb{E}[\|\Delta w_{i,t}^\theta\|^2] \leq \eta^2 S \sum_{s=0}^{S-1} \mathbb{E}[\|g_{i,t,s}\|^2] \leq \eta^2 S^2 G^2. \quad (63)$$

Combining (59) and (63), we obtain

$$\mathbb{E}[\|\mathbf{p}_{i,t}^c - \mathbf{p}_{i,t-1}^c\|^2] \leq L_{w^\theta}^2 \eta^2 S^2 G^2. \quad (64)$$

Part (a): per-client bound. For a fixed client i , the Frobenius norm of its prototype matrix satisfies

$$\|\mathbf{P}_{i,t} - \mathbf{P}_{i,t-1}\|_F^2 = \sum_{c \in \mathcal{C}_i} \|\mathbf{p}_{i,t}^c - \mathbf{p}_{i,t-1}^c\|^2. \quad (65)$$

Taking expectations and applying the bound above,

$$\begin{aligned} \mathbb{E}[\|\mathbf{P}_{i,t} - \mathbf{P}_{i,t-1}\|_F^2] &\leq \sum_{c \in \mathcal{C}_i} L_{w^\theta}^2 \eta^2 S^2 G^2 \\ &= C_i L_{w^\theta}^2 \eta^2 S^2 G^2. \end{aligned} \quad (66)$$

Using Jensen's inequality, we obtain

$$\begin{aligned} \mathbb{E}[\|\mathbf{P}_{i,t} - \mathbf{P}_{i,t-1}\|_F] &\leq \sqrt{\mathbb{E}[\|\mathbf{P}_{i,t} - \mathbf{P}_{i,t-1}\|_F^2]} \\ &\leq L_{w^\theta} \eta S G \sqrt{C_i} =: k_i \eta S G. \end{aligned} \quad (67)$$

which yields (52). Since $C_i \leq C_{\max}$ for every i , set $k_{\max} := L_{w^\theta} \sqrt{C_{\max}}$; then $k_i \leq k_{\max}$.

Part (b): global bound. The stacked prototype matrix is $\mathbf{P}_t := \{\mathbf{P}_{i,t}\}_{i=1}^N$. Taking expectations and using the per-client bound,

$$\begin{aligned} \mathbb{E}[\|\Delta \mathbf{P}_t\|_F^2] &\leq \sum_{i=1}^N C_i L_{w^\theta}^2 \eta^2 S^2 G^2 \\ &= L_{w^\theta}^2 \eta^2 S^2 G^2 \sum_{i=1}^N C_i. \end{aligned} \quad (68)$$

Again by Jensen inequality,

$$\begin{aligned} \mathbb{E}[\|\Delta \mathbf{P}_t\|_F] &\leq \sqrt{\mathbb{E}[\|\Delta \mathbf{P}_t\|_F^2]} \\ &\leq L_{w^\theta} \eta S G \sqrt{\sum_{i=1}^N C_i} =: k_{\text{glob}} \eta S G. \end{aligned} \quad (69)$$

Finally, since $C_i \leq C_{\max}$ for all i , we have

$$\sum_{i=1}^N C_i \leq \sum_{i=1}^N C_{\max} = N C_{\max}, \quad (70)$$

so $k_{\text{glob}} \leq L_{w^\theta} \sqrt{N C_{\max}}$. This proves part (b) and completes the proof. \square

Lemma 3 (Loss change due to prototype refresh). *Define*

$$\mathcal{L}_{i,t}(w) := \mathcal{L}_{\text{ce},i}(w) + \lambda_t \Phi_i(w; \mathbf{Q}_{t-1}, \mathbf{P}_{t-1}), \quad (71)$$

$$\mathcal{L}_{i,t+1}(w) := \mathcal{L}_{\text{ce},i}(w) + \lambda_{t+1} \Phi_i(w; \mathbf{Q}_t, \mathbf{P}_t). \quad (72)$$

Under Assumptions 4 and 5, for any client i ,

$$\begin{aligned} \mathbb{E}[\|\mathcal{L}_{i,t+1}(w_{i,t,S}) - \mathcal{L}_{i,t}(w_{i,t,S})\|] &\leq |\lambda_{t+1} - \lambda_t| B_\Phi \\ &\quad + \lambda_{t+1} \Gamma(\tau) k_{\text{glob}} \eta S G, \end{aligned} \quad (73)$$

where $\Gamma(\tau) := c_\Phi(\tau)(1 + L_{\text{agg}}(\tau))$ and k_{glob} is as in Lemma 2(b).

Proof. Fix a client i and a round $t \geq 1$. We want to control the difference between the objectives at rounds t and $t+1$ when both are evaluated at the same parameter vector $w_{i,t,S}$, namely $\mathcal{L}_{i,t+1}(w_{i,t,S}) - \mathcal{L}_{i,t}(w_{i,t,S})$.

a) *Step 1: Separate schedule and prototype effects.*: By definitions (71) and (72), for any w we have. For conciseness, introduce the shorthand

$$\Phi_{i,\tau}(w) := \Phi_i(w; \mathbf{Q}_\tau, \mathbf{P}_\tau) \quad (74)$$

for any round index τ ; we will only need $\Phi_{i,t}$ and $\Phi_{i,t-1}$ below.

$$\begin{aligned} \mathcal{L}_{i,t+1}(w) - \mathcal{L}_{i,t}(w) &= \mathcal{L}_{\text{ce},i}(w) + \lambda_{t+1}\Phi_{i,t}(w) \\ &\quad - \mathcal{L}_{\text{ce},i}(w) - \lambda_t\Phi_{i,t-1}(w) \\ &= \lambda_{t+1}\Phi_{i,t}(w) - \lambda_t\Phi_{i,t-1}(w). \end{aligned}$$

Add and subtract the term $\lambda_{t+1}\Phi_i(w; \mathbf{Q}_{t-1}, \mathbf{P}_{t-1})$ to get

$$\begin{aligned} \mathcal{L}_{i,t+1}(w) - \mathcal{L}_{i,t}(w) &= (\lambda_{t+1} - \lambda_t)\Phi_{i,t-1}(w) \\ &\quad + \lambda_{t+1}(\Phi_{i,t}(w) - \Phi_{i,t-1}(w)). \end{aligned} \quad (75)$$

We now bound these two parts separately.

b) *Step 2: Bound the schedule-change term.*: Take absolute values in (75):

$$\begin{aligned} |\mathcal{L}_{i,t+1}(w) - \mathcal{L}_{i,t}(w)| &\leq |\lambda_{t+1} - \lambda_t| |\Phi_{i,t-1}(w)| \\ &\quad + \lambda_{t+1} |\Phi_{i,t}(w) - \Phi_{i,t-1}(w)|. \end{aligned} \quad (76)$$

By Assumption 5(A5.2), the prototype-based regularizer is uniformly bounded:

$$0 \leq \Phi_i(w; \mathbf{Q}, \mathbf{P}) \leq B_\Phi \quad \text{for all } w, \mathbf{Q}, \mathbf{P}. \quad (77)$$

Hence, for the first term in (76) we have

$$|\lambda_{t+1} - \lambda_t| |\Phi_{i,t-1}(w)| \leq |\lambda_{t+1} - \lambda_t| B_\Phi. \quad (78)$$

c) *Step 3: Bound the prototype-refresh term via Lipschitz properties.*: For the second term in (76), apply Assumption 5(A5.1), which states that Φ_i is Lipschitz in (\mathbf{Q}, \mathbf{P}) . Define the shorthand differences

$$\Delta \mathbf{Q}_t := \mathbf{Q}_t - \mathbf{Q}_{t-1}, \quad \Delta \mathbf{P}_t := \mathbf{P}_t - \mathbf{P}_{t-1}. \quad (79)$$

Then

$$\begin{aligned} |\Phi_i(w; \mathbf{Q}_t, \mathbf{P}_t) - \Phi_i(w; \mathbf{Q}_{t-1}, \mathbf{P}_{t-1})| \\ \leq c_\Phi(\tau) \left(\|\Delta \mathbf{Q}_t\|_F \right. \\ \left. + \|\Delta \mathbf{P}_t\|_F \right). \end{aligned} \quad (80)$$

We now relate $\|\mathbf{Q}_t - \mathbf{Q}_{t-1}\|_F$ to $\|\mathbf{P}_t - \mathbf{P}_{t-1}\|_F$ by using Assumption 4 (Lipschitz personalized aggregation):

$$\|\Delta \mathbf{Q}_t\|_F = \|\mathbf{Q}_\tau(\mathbf{P}_t) - \mathbf{Q}_\tau(\mathbf{P}_{t-1})\|_F \leq L_{\text{agg}}(\tau) \|\Delta \mathbf{P}_t\|_F. \quad (81)$$

Substituting (81) into (80) gives

$$\begin{aligned} |\Phi_i(w; \mathbf{Q}_t, \mathbf{P}_t) - \Phi_i(w; \mathbf{Q}_{t-1}, \mathbf{P}_{t-1})| \\ \leq c_\Phi(\tau) \left(L_{\text{agg}}(\tau) \|\Delta \mathbf{P}_t\|_F \right. \\ \left. + \|\Delta \mathbf{P}_t\|_F \right) \\ = c_\Phi(\tau) (1 + L_{\text{agg}}(\tau)) \|\Delta \mathbf{P}_t\|_F. \end{aligned}$$

Define

$$\Gamma(\tau) := c_\Phi(\tau) (1 + L_{\text{agg}}(\tau)), \quad (82)$$

so that

$$\begin{aligned} |\Phi_i(w; \mathbf{Q}_t, \mathbf{P}_t) - \Phi_i(w; \mathbf{Q}_{t-1}, \mathbf{P}_{t-1})| \\ \leq \Gamma(\tau) \|\Delta \mathbf{P}_t\|_F. \end{aligned} \quad (83)$$

Multiplying (83) by λ_{t+1} yields

$$\begin{aligned} \lambda_{t+1} |\Phi_i(w; \mathbf{Q}_t, \mathbf{P}_t) - \Phi_i(w; \mathbf{Q}_{t-1}, \mathbf{P}_{t-1})| \\ \leq \lambda_{t+1} \Gamma(\tau) \|\Delta \mathbf{P}_t\|_F. \end{aligned} \quad (84)$$

d) *Step 4: Combine bounds and evaluate at $w_{i,t,S}$.*

Define the per-round loss change

$$\Delta \mathcal{L}_{i,t}(w) := \mathcal{L}_{i,t+1}(w) - \mathcal{L}_{i,t}(w). \quad (85)$$

Substitute (78) and (84) into (76):

$$\begin{aligned} |\Delta \mathcal{L}_{i,t}(w)| &\leq |\lambda_{t+1} - \lambda_t| B_\Phi \\ &\quad + \lambda_{t+1} \Gamma(\tau) \|\Delta \mathbf{P}_t\|_F. \end{aligned} \quad (86)$$

Now set $w = w_{i,t,S}$, the parameters after the S local steps in round t :

$$\begin{aligned} |\Delta \mathcal{L}_{i,t}(w_{i,t,S})| &\leq |\lambda_{t+1} - \lambda_t| B_\Phi \\ &\quad + \lambda_{t+1} \Gamma(\tau) \|\Delta \mathbf{P}_t\|_F. \end{aligned} \quad (87)$$

e) *Step 5: Take expectations and use the prototype-movement bound.*: Finally, take expectations on both sides of (87):

$$\begin{aligned} \mathbb{E} \left[|\Delta \mathcal{L}_{i,t}(w_{i,t,S})| \right] &\leq |\lambda_{t+1} - \lambda_t| B_\Phi \\ &\quad + \lambda_{t+1} \Gamma(\tau) \mathbb{E} [\|\Delta \mathbf{P}_t\|_F]. \end{aligned} \quad (88)$$

By Lemma 2(b) in its causal form, the stacked prototype movement is bounded by

$$\mathbb{E} [\|\Delta \mathbf{P}_t\|_F] \leq k_{\text{glob}} \eta S G. \quad (89)$$

Substituting (89) into (88) gives

$$\begin{aligned} \mathbb{E} \left[|\Delta \mathcal{L}_{i,t}(w_{i,t,S})| \right] &\leq |\lambda_{t+1} - \lambda_t| B_\Phi \\ &\quad + \lambda_{t+1} \Gamma(\tau) k_{\text{glob}} \eta S G, \end{aligned} \quad (90)$$

which is exactly (73). This completes the proof. \square

We now connect round t and round $t+1$ for client i .

Theorem 1 (One-round deviation for an arbitrary client). *Let Assumptions 1 to 5 hold. For any client i and any $t \geq 1$, with stepsize $0 < \eta \leq 1/L_t$, we have*

$$\begin{aligned} \mathbb{E} [\mathcal{L}_{i,t+1}(w_{i,t+1,0})] &\leq \mathbb{E} [\mathcal{L}_{i,t}(w_{i,t,0})] - \frac{\eta}{2} G_{i,t}^2 \\ &\quad + \frac{L_t \eta^2}{2} S \sigma^2 + \lambda_{t+1} \Gamma(\tau) k_{\text{glob}} \eta S G \\ &\quad + |\lambda_{t+1} - \lambda_t| B_\Phi. \end{aligned} \quad (91)$$

Proof. By Corollary 1 and the bound $\eta \leq 1/L_t$, we have $1 - \frac{L_t \eta}{2} \geq \frac{1}{2}$, so

$$\mathbb{E} [\mathcal{L}_{i,t}(w_{i,t,S})] \leq \mathbb{E} [\mathcal{L}_{i,t}(w_{i,t,0})] - \frac{\eta}{2} G_{i,t}^2 + \frac{L_t \eta^2}{2} S \sigma^2. \quad (92)$$

By definition $w_{i,t+1,0} := w_{i,t,S}$, and

$$\mathbb{E} [\mathcal{L}_{i,t+1}(w_{i,t+1,0})] = \mathbb{E} [\mathcal{L}_{i,t+1}(w_{i,t,S})]. \quad (93)$$

Add and subtract $\mathcal{L}_{i,t}(w_{i,t,S})$ inside the expectation:

$$\begin{aligned} \mathbb{E} [\mathcal{L}_{i,t+1}(w_{i,t,S})] &= \mathbb{E} [\mathcal{L}_{i,t}(w_{i,t,S})] \\ &\quad + \mathbb{E} [\mathcal{L}_{i,t+1}(w_{i,t,S}) - \mathcal{L}_{i,t}(w_{i,t,S})]. \end{aligned} \quad (94)$$

Apply Lemma 3:

$$\mathbb{E}[\mathcal{L}_{i,t+1}(w_{i,t,S}) - \mathcal{L}_{i,t}(w_{i,t,S})] \leq |\lambda_{t+1} - \lambda_t| B_\Phi + \lambda_{t+1} \Gamma(\tau) k_{\text{glob}} \eta S G. \quad (95)$$

Combining (94) and (95), we obtain

$$\begin{aligned} \mathbb{E}[\mathcal{L}_{i,t+1}(w_{i,t+1,0})] &= \mathbb{E}[\mathcal{L}_{i,t+1}(w_{i,t,S})] \\ &\leq \mathbb{E}[\mathcal{L}_{i,t}(w_{i,t,S})] \\ &\quad + |\lambda_{t+1} - \lambda_t| B_\Phi \\ &\quad + \lambda_{t+1} \Gamma(\tau) k_{\text{glob}} \eta S G. \end{aligned} \quad (96)$$

Finally, plug (92) into (96) to eliminate $\mathcal{L}_{i,t}(w_{i,t,S})$:

$$\begin{aligned} \mathbb{E}[\mathcal{L}_{i,t+1}(w_{i,t+1,0})] &\leq \mathbb{E}[\mathcal{L}_{i,t}(w_{i,t,0})] - \frac{\eta}{2} G_{i,t}^2 + \frac{L_t \eta^2}{2} S \sigma^2 \\ &\quad + |\lambda_{t+1} - \lambda_t| B_\Phi \\ &\quad + \lambda_{t+1} \Gamma(\tau) k_{\text{glob}} \eta S G, \end{aligned} \quad (97)$$

which is exactly (91). This completes the proof. \square

Building on Theorem 1, we have the following overall convergence guarantee after the warm-up phase.

Theorem 2 (ε -stationarity after warm-up). *Suppose Assumptions 1 to 6 hold and that $\lambda_t \equiv \lambda$ and $L_t \leq L_{\max}$ for all $t \geq T_{\text{warm}}$. We consider T communication rounds after T_{warm} ; for notational convenience, we re-index these rounds as $t \in 1, \dots, T$. Each round has S local steps, so there are $K := TS$ total local updates in this phase. For any client i , the iterates of FedAPA satisfy*

$$\begin{aligned} \frac{1}{K} \sum_{t=1}^T G_{i,t}^2 &\leq \frac{2\Delta_i}{K\eta} \\ &\quad + L_{\max} \eta \sigma^2 + 2\lambda \Gamma(\tau) k_{\text{glob}} G, \end{aligned} \quad (98)$$

for any stepsize $0 < \eta \leq 1/L_{\max}$, where

$$\Delta_i := \mathbb{E}[\mathcal{L}_{i,T_{\text{warm}}}(w_{i,T_{\text{warm}},0})] - L_{\text{inf}}, \quad (99)$$

$$\Gamma(\tau) := c_\Phi(\tau)(1 + L_{\text{agg}}(\tau)), \quad (100)$$

and k_{glob} is the prototype-movement constant from Lemma 2(b).

Moreover, for any target $\varepsilon > 0$, if the parameters satisfy

$$0 < \eta \leq \min \left\{ \frac{1}{L_{\max}}, \frac{\varepsilon}{3L_{\max}\sigma^2} \right\}, \quad (101)$$

$$\lambda \leq \frac{\varepsilon}{6\Gamma(\tau)k_{\text{glob}}G}, \quad (102)$$

$$T \geq \frac{6\Delta_i}{\varepsilon\eta S}, \quad (103)$$

then FedAPA achieves ε -stationarity for client i :

$$\frac{1}{K} \sum_{t=1}^T G_{i,t}^2 \leq \varepsilon. \quad (104)$$

The bound in (98) shows that, for each client i , the last term $2\lambda\Gamma(\tau)k_{\text{glob}}G$ forms an asymptotic error floor due to prototype refresh: for fixed $\lambda > 0$, the first two terms can be made arbitrarily small by taking K large and η small, but the floor remains. Our ε -stationarity result is obtained by choosing η , T , and λ so that each term is at most $\varepsilon/3$, as in (101) to (103); in particular, this requires $\lambda = O(\varepsilon/(\Gamma(\tau)k_{\text{glob}}G))$.

The dependence on similarity-weighted prototypes appears only through the factor $\lambda\Gamma(\tau)k_{\text{glob}}$. Our analysis assumes a finite constant $\Gamma(\tau)$ for each τ . Intuitively, larger τ makes the softmax weights flatter and the aggregation less sensitive to prototype differences, which can reduce $\Gamma(\tau)$ in practice, although such monotonic behavior is not required or proved by the theorem.

Proof. Fix a client i and consider the T rounds after T_{warm} , where $\lambda_t \equiv \lambda$ and $L_t \leq L_{\max}$. For notational simplicity, we re-index these rounds as $t = 1, \dots, T$. We write

$$\mathcal{L}_{i,t} := \mathcal{L}_{i,t}(w_{i,t,0}). \quad (105)$$

Step 1: One-round inequality after warm-up.

From Theorem 1, using $\lambda_{t+1} = \lambda_t = \lambda$ for all $t \geq T_{\text{warm}}$ so that the schedule-change term vanishes, and using $L_t \leq L_{\max}$, we obtain for each $t \geq T_{\text{warm}}$:

$$\begin{aligned} \mathbb{E}[\mathcal{L}_{i,t+1}] &\leq \mathbb{E}[\mathcal{L}_{i,t}] - \frac{\eta}{2} G_{i,t}^2 + \frac{L_{\max}\eta^2}{2} S \sigma^2 \\ &\quad + \lambda \Gamma(\tau) k_{\text{glob}} \eta S G. \end{aligned} \quad (106)$$

Step 2: Telescoping over T rounds.

Sum (106) from $t = T_{\text{warm}}$ to $T_{\text{warm}} + T - 1$:

$$\begin{aligned} \mathbb{E}[\mathcal{L}_{i,T_{\text{warm}}+T}] &\leq \mathbb{E}[\mathcal{L}_{i,T_{\text{warm}}}] - \frac{\eta}{2} \sum_t G_{i,t}^2 + \frac{L_{\max}\eta^2}{2} T S \sigma^2 \\ &\quad + T \lambda \Gamma(\tau) k_{\text{glob}} \eta S G. \end{aligned} \quad (107)$$

Rearrange:

$$\begin{aligned} \frac{\eta}{2} \sum_t G_{i,t}^2 &\leq \mathbb{E}[\mathcal{L}_{i,T_{\text{warm}}}] - \mathbb{E}[\mathcal{L}_{i,T_{\text{warm}}+T}] \\ &\quad + \frac{L_{\max}\eta^2}{2} T S \sigma^2 + T \lambda \Gamma(\tau) k_{\text{glob}} \eta S G. \end{aligned} \quad (108)$$

By Assumption 1, $\mathcal{L}_{i,t}(w) \geq L_{\text{inf}}$, so $\mathbb{E}[\mathcal{L}_{i,T_{\text{warm}}+T}] \geq L_{\text{inf}}$. Define

$$\Delta_i := \mathbb{E}[\mathcal{L}_{i,T_{\text{warm}}}] - L_{\text{inf}} \geq 0. \quad (109)$$

Then (108) yields

$$\frac{\eta}{2} \sum_t G_{i,t}^2 \leq \Delta_i + \frac{L_{\max}\eta^2}{2} T S \sigma^2 + T \lambda \Gamma(\tau) k_{\text{glob}} \eta S G. \quad (110)$$

Step 3: Normalize by $K = TS$.

Recall that

$$\sum_t G_{i,t}^2 = \sum_{t=1}^T \sum_{s=0}^{S-1} \mathbb{E}[\|\nabla \mathcal{L}_{i,t}(w_{i,t,s})\|^2], \quad (111)$$

and $K := TS$. Divide by K :

$$\begin{aligned} \frac{\eta}{2} \cdot \frac{1}{K} \sum_{t=1}^T \sum_{s=0}^{S-1} \mathbb{E}[\|\nabla \mathcal{L}_{i,t}(w_{i,t,s})\|^2] &\leq \frac{\Delta_i}{K} + \frac{L_{\max}\eta^2}{2} \sigma^2 \\ &\quad + \lambda \Gamma(\tau) k_{\text{glob}} \eta G. \end{aligned} \quad (112)$$

Multiply both sides by $2/\eta$ to obtain (98).

Step 4: Enforce the ε -conditions.

Let $\varepsilon > 0$ be given.

(i) The step size constraint (101) ensures

$$L_{\max}\eta\sigma^2 \leq \frac{\varepsilon}{3}. \quad (113)$$

(ii) The prototype weight condition (102) ensures

$$2\lambda\Gamma(\tau)k_{\text{glob}}G \leq \frac{\varepsilon}{3}. \quad (114)$$

(iii) If we take (103) so that $K = TS \geq 6\Delta_i/(\varepsilon\eta)$, then

$$\frac{2\Delta_i}{K\eta} \leq \frac{\varepsilon}{3}. \quad (115)$$

Substituting these three bounds into (98) yields

$$\frac{1}{K} \sum_{t=1}^T \sum_{s=0}^{S-1} \mathbb{E}[\|\nabla \mathcal{L}_{i,t}(w_{i,t,s})\|^2] \leq \frac{\varepsilon}{3} + \frac{\varepsilon}{3} + \frac{\varepsilon}{3} = \varepsilon, \quad (116)$$

which completes the proof. \square